Взаимодействие коротких интенсивных лазерных импульсов с веществом: вторичные источники излучения и быстрых частиц

Н.Е. Андреев

Institute for High Energy Densities
Joint Institute for High Temperatures
Russian Academy of Sciences, Moscow, Russia

Лаборатория 1.5.2 НИЦ-1 ТЭС

Ученый Совет ОИВТ
12 декабря 2011 г.

PW-class lasers: MJ in nanosecond pulses: 10^6 J / 10^{-9} s = 10^{15} W

NIF is the world's largest and most energetic laser: 2.0 MJ, 192 beams

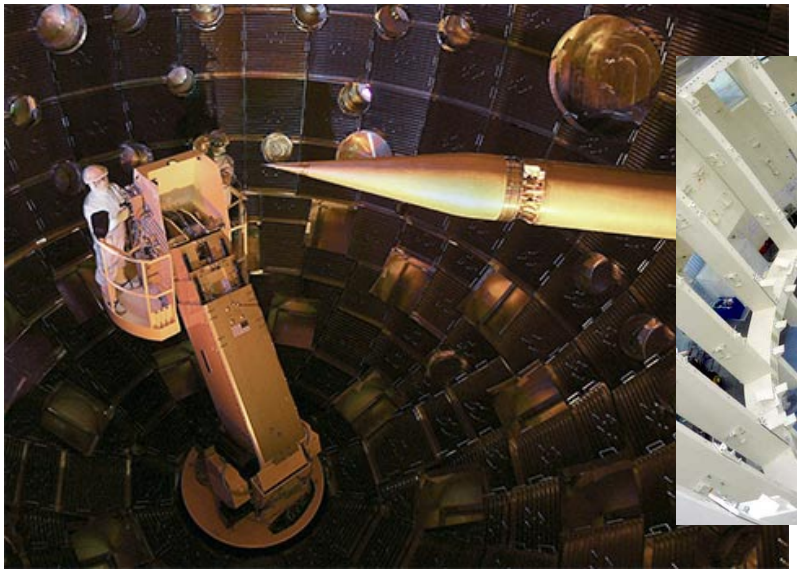

Laser Mégajoule plans to deliver about 1.8 MJ of laser energy, 240 beams

PW-class lasers: 30 J in 30 fs single pulse : 30 J / 30×10^{-15} s = 10^{15} W

HERCULES holds world records for the highest focused intensity, 2×10^{22} Wcm^{-2}

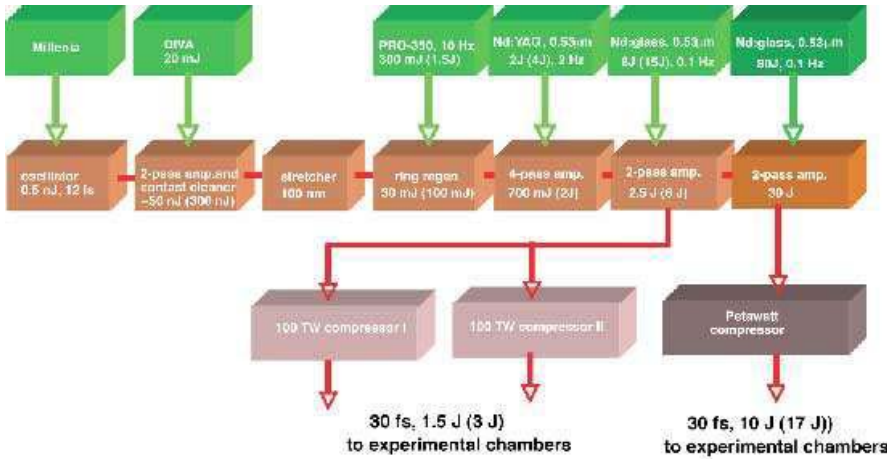

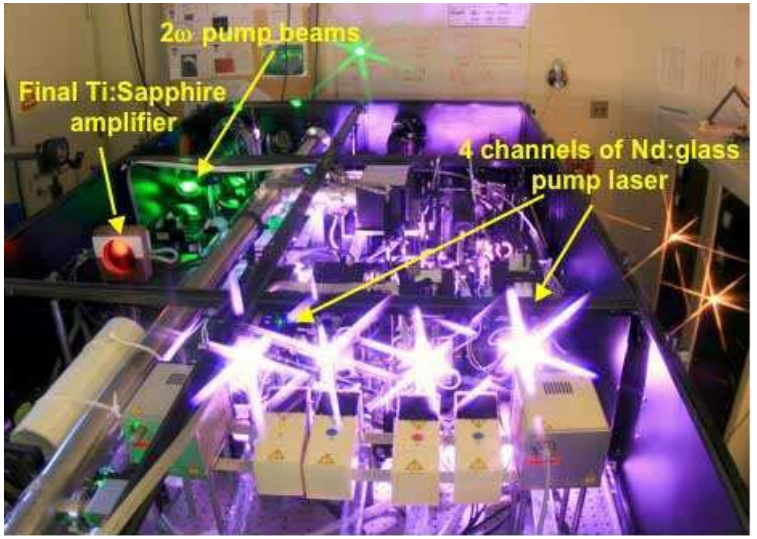

The goal of FOCUS High-Field is to explore the ultra-relativistic intensity regime of laser-matter interaction, and ultimately reach 10^{23} W/cm^2, by focusing about 15 J at 30 fsec (500 TW) to a diffraction limited focal spot of about 1 micron

Chirped Pulse Amplification

D. Strickland and G. Mourou 1985

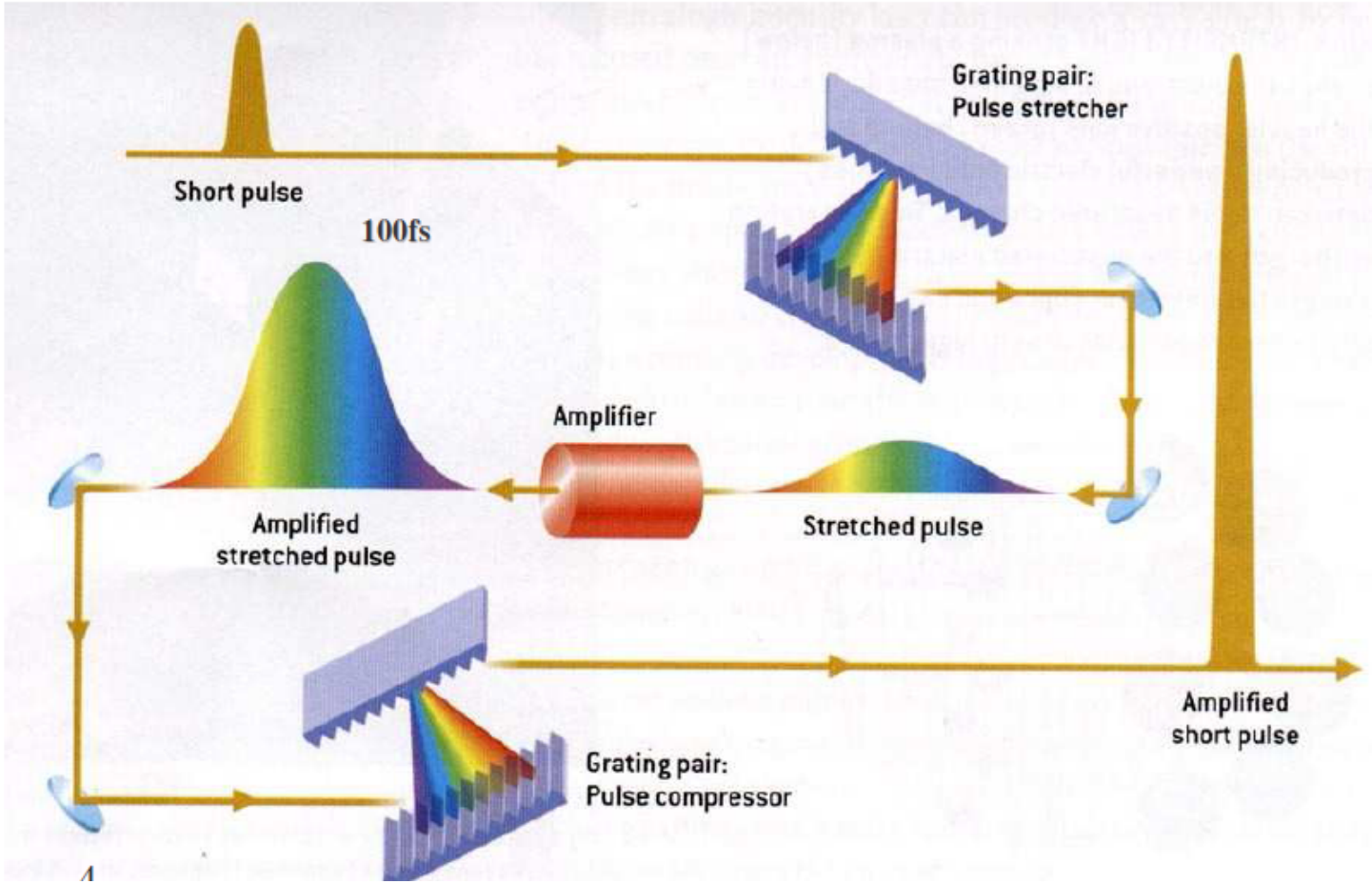

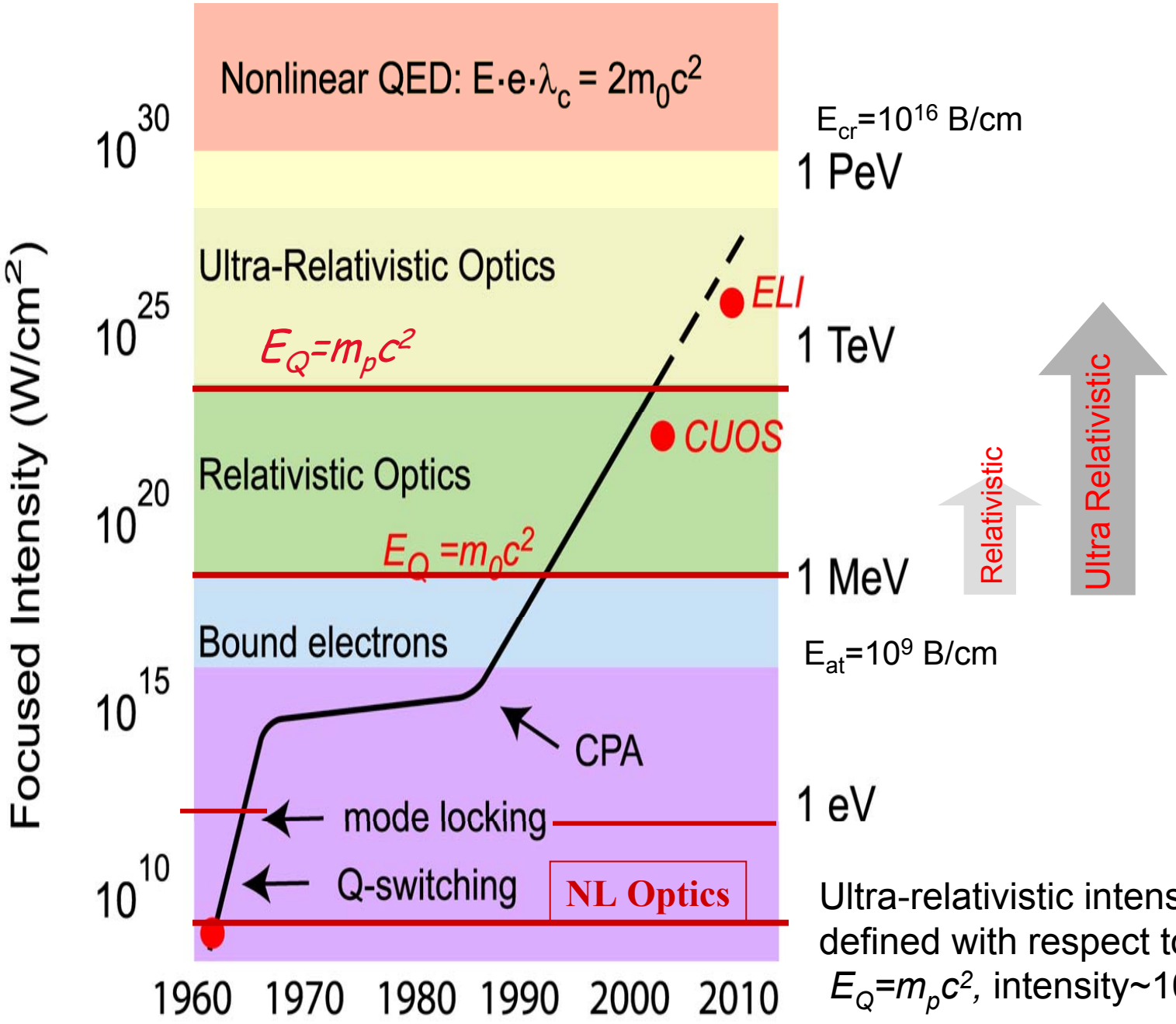

Ultra-relativistic intensity is defined with respect to the proton $E_Q=m_pc^2$, intensity~10^{24}W/cm^2

Фемтосекундный лазерный комплекс ОИВТ

Femtosecond Terawatt Ti:Sapphire Laser System
800 nm; 40 fs; 10 Hz, to 10 TW

Focused intensity 10^{19} W/cm^2

Terawatt femtosecond Cr- forsterite laser system
1240 nm; 80 fs; 90 mJ; 10 Hz
(made in Russia)

Вторичные источники излучения

K_α radiation of solids by short intense laser pulses

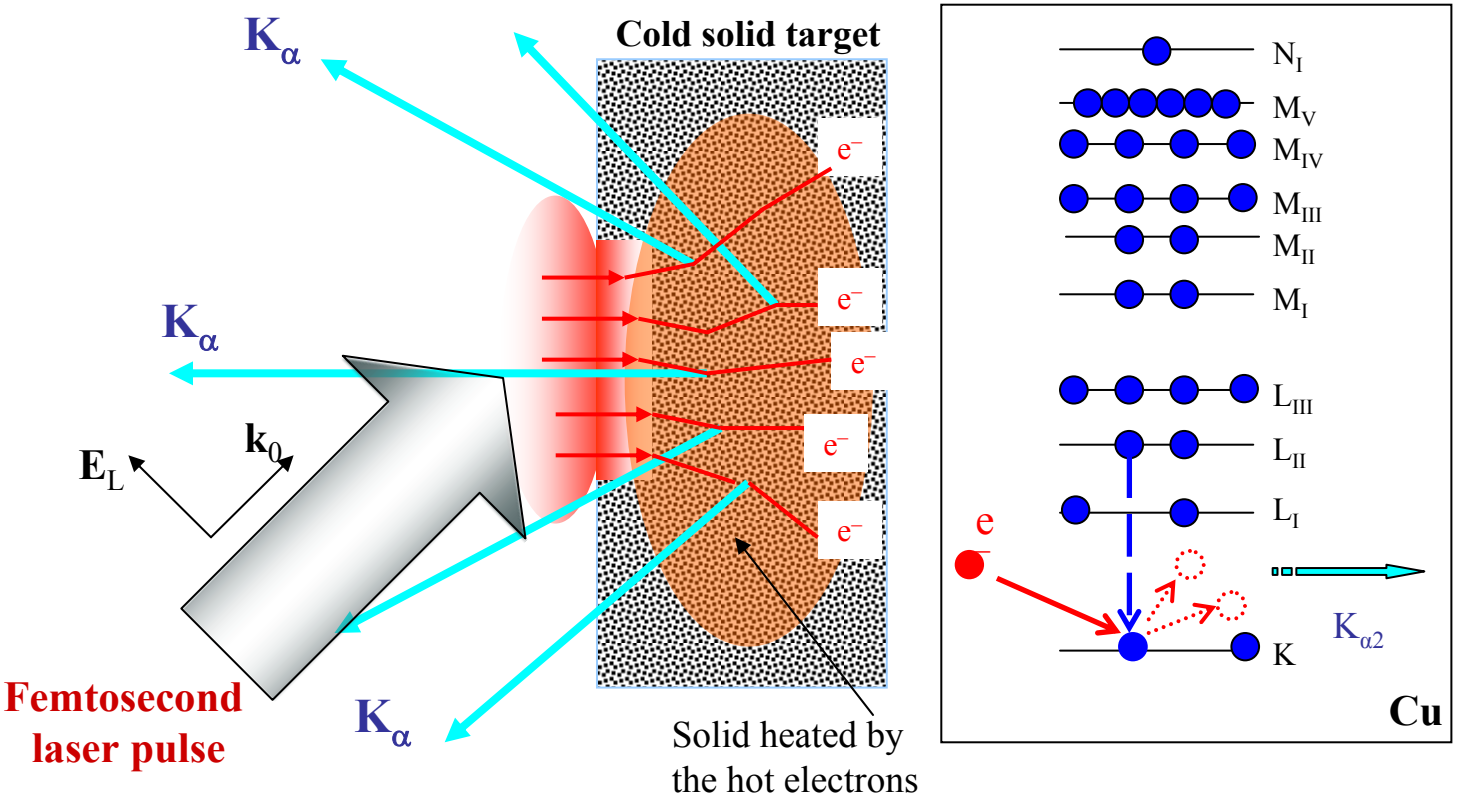

K_a radiation of solids by short intense laser pulses

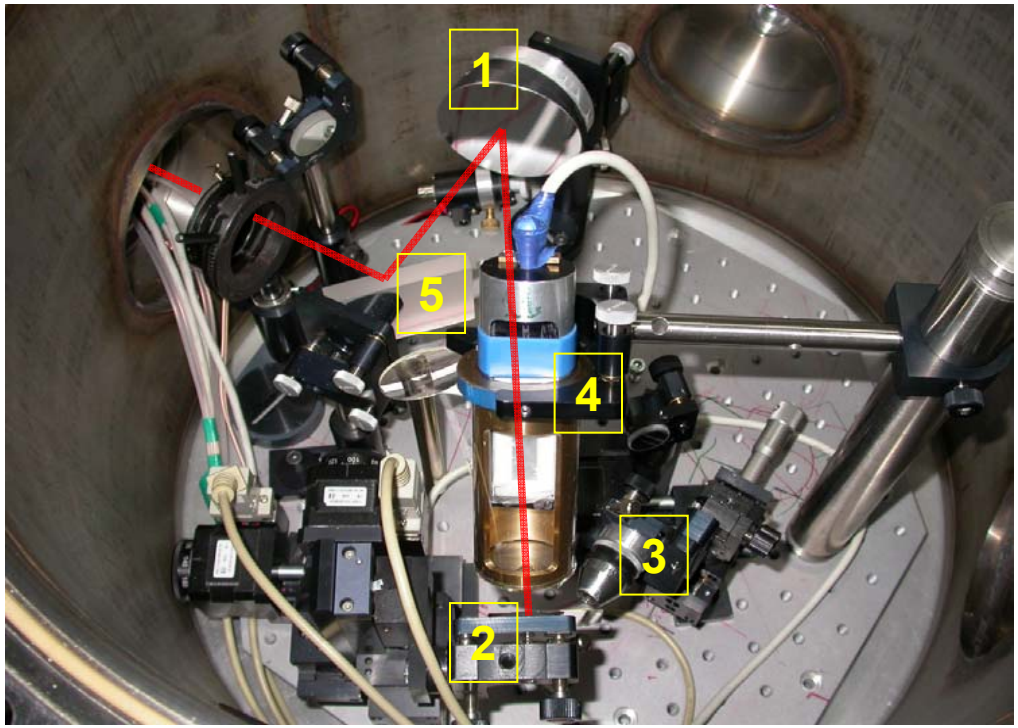

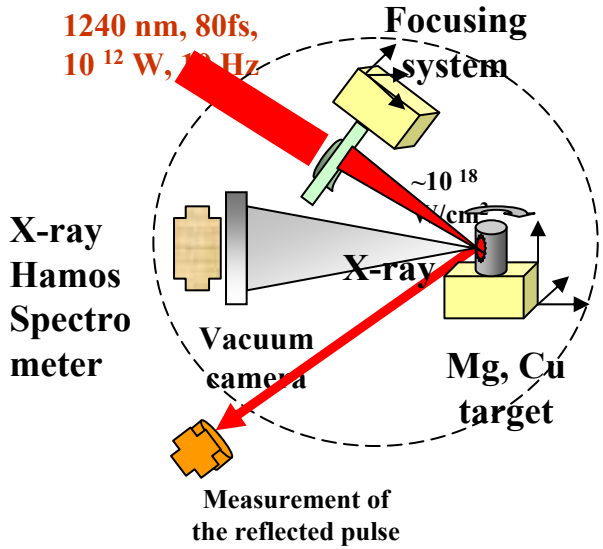

1 - Off-axis paraboloid (focal length 254mm).
2 - Motorized target unit with target holder.
3 - System for interactive control of focus spot.
4 – Von Hamos spectrometer
5 – Mirror (R=100%)

Focal spot

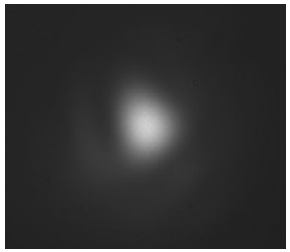

$D_{1/e}$=14μm

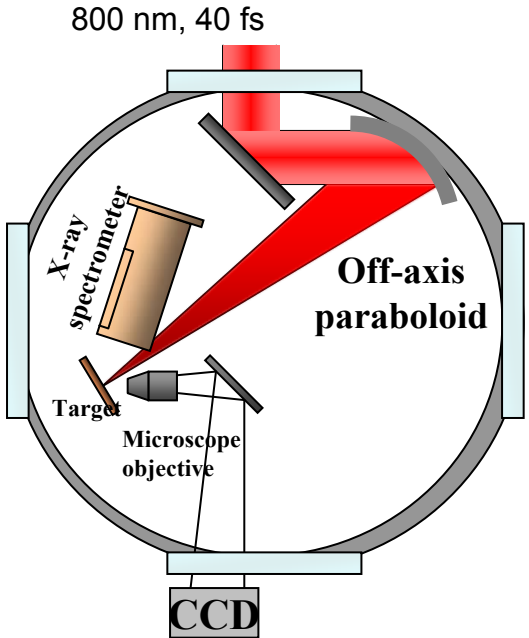

M. B. Agranat, N. E. Andreev, S. I. Ashitkov, A. V. Ovchinnikov, D. S. Sitnikov, V. E. Fortov, A. P. Shevelko, Generation of Ka radiation by a forsterite terawatt laser, JETP Lett. 83, 72 (2006)

X-ray radiation using solid targets

K_α radiation from Cu laser-produced plasmas
Cr:Forsterite laser system, ω_0, *p-polarization*,
E_L=30 mJ, τ_L = 80 fs, $10^{16} \div 10^{17}$ W/cm^2

Single laser short experiment

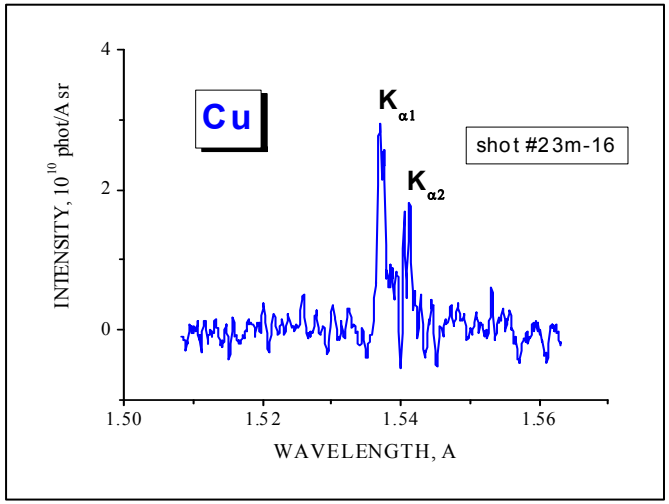

$$E_0 = E_L\left[1+(1-f)^{1/2}\right]\sin\theta$$

$$T_{h,keV} = 7.6 I_{L,16}\lambda^2_{\mu m}\alpha^2\sin^2\theta$$

Optimization of K_α x-ray yield

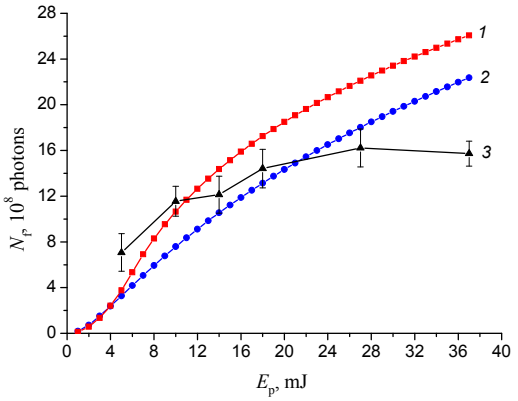

The model calculation of K_α yield against pulse energy in comparison with experimental data received at IHED laser facility:
λ = 1.24 μm, τ_p = 80 fs,
d_f = 10 μm, θ = 45°, Fe target

E_0 – driving, E_L – laser field, f –absorption,
η = 1.57, $I_{L,16} = I_L/10^{16}$ W/cm^2 – laser intensity

There is a range of laser pulse parameters where K_α yield is described by **vacuum heating mechanism**

РОССИЙСКАЯ АКАДЕМИЯ НАУК
Физический институт имени П.Н.Лебедева
Ф И А Н
117924, ГСП-1, Москва, В-333
Ленинский просп. 53,
Для телеграмм: Москва В-333 ФИАН
Телекс: Москва 113308 НЕОДИМ
Факс: (095) 938 22 51
Tel.: (095) 135 14 29

[1] Kostenko O.F., Andreev N.E. (2011) *Plasma Phys. Rep.* V. 37. P. 433.
[2] Agranat M.B., Andreev N.E., Ashitkov S.I. et al. (2006) *JETP Letters* V. 83. P. 72.

X-ray radiation using nano-structured targets

Fe clusters on Cu target

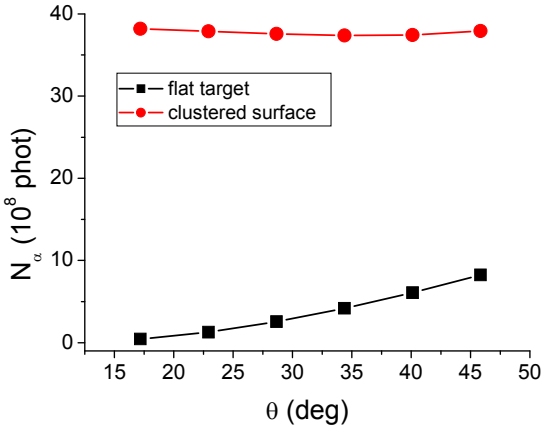

Dependence of K_α yield on angle of incidence for peak intensity 3×10^{17} W/cm^2

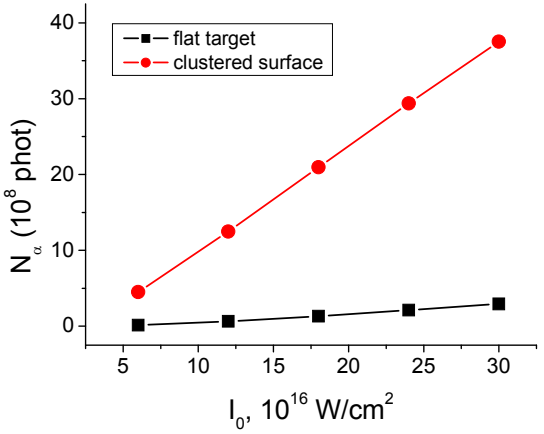

Dependence of K_α yield on peak intensity for angle of incidence 30°

$$E_0 = 3E_L \cos\theta_1$$

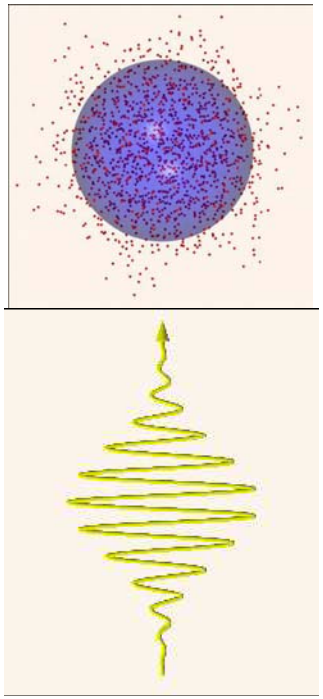

$$T_{h,keV} = 68.41 \times I_{L,16}\lambda^2_{\mu m}\cos^2\theta_1$$

Enhancement of driving electric field at a cluster surface and favorable conditions for K_α photons to escape from the wafer lead to considerable enhancement of K_α yield

Comparison of the theory with measurements

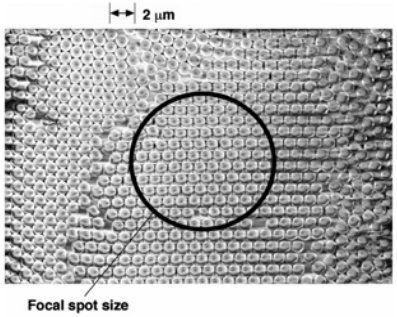

Fig. 1. Scanning electron microscope image of 1 μm diameter polystyrene spheres arrayed on a Cu substrate [1].

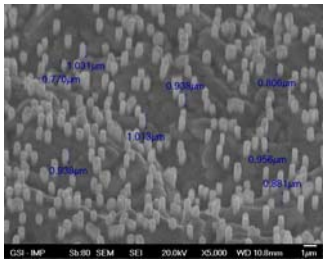

Fig. 3. The nano-rods (about 10^8 rods/cm^2) each of 500 nm in diameter and about 1 μm of height, which supported by the 8 μm thick Cu layer [3].

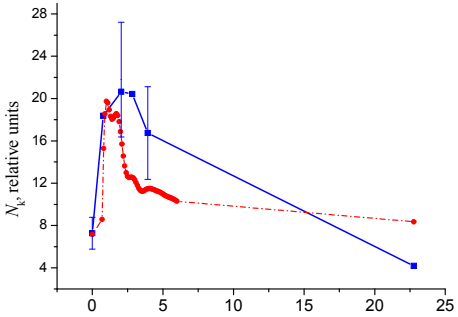

Fig. 2. Relative enhancement of K_α yield from Si wafer with $I_L = 2\times10^{17}$ W/cm^2, $\lambda = 0.4$ μm and $\theta = 45°$. The experiment [1] (blue line) and the theory [2] (red line).

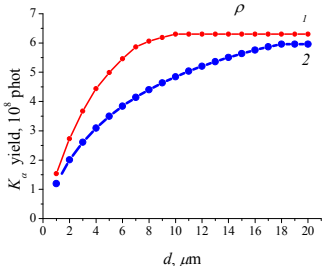

Fig. 4. K_α yield vs polished copper foil thickness. Curve *1* is for Brunel distribution, and curve *2* is for corresponding Maxwellian distribution of hot electrons. $I_L = 1.4\times10^{17}$ W/cm^2, $\theta = 45°$, $\lambda = 0.8$ μm, $\tau_L = 40$ fs, $r_f = 7$ μm.

The number of photons generated by an electron incident upon a foil of thickness d is $N_g = N_{g0} U\left(\frac{d - l_k(\varepsilon)\cos\chi}{l_\gamma}\right)$,

where N_{g0} is the number of photons into 2π solid angle generated in a solid target by an electron of energy E, $l_k(\varepsilon)$ is the mean depth of K_α generation, $\varepsilon = E/I_k$, where I_k is the K-shell ionization energy, l_γ is the absorption length for self-emitted K_α radiation, χ is an angle of incidence of the electron, U is a step function.

Calculations for a Si wafer covered with spherical clusters (Fig. 1) exhibited satisfactory agreement with measurements of the relative enhancement of K_α yield in the range $\rho \approx 1$–4 (Fig. 2).

Measured relative increase in x-ray yield from the foil covered with metal rods of submicron sizes, with low aspect ratio (Fig. 3), is best fitted by half-spherical clusters with diameter which equals to the initial diameter of the rods.

Calculations with Maxwellian distribution of hot electrons (Fig. 4) reproduce well the relative increase of K_α emission with increase of the polished foil thickness.

[1] Sumeruk H.A. et al. (2007) *Phys. Rev. Lett.* V. 98. P. 045001.
[2] Kostenko O.F., Andreev N.E. (2010) *Phys. Scr.* V. 81. P. 055505.
[3] Ovchinnikov A.V., Kostenko O.F., Chefonov O.V., Rosmej O.N., Andreev N.E., Agranat M.B., Duan J.L., Liu J., and Fortov V.E. (2011) *Laser Part. Beams* V. 29. P. 249.

Вторичные источники излучения

Генерация терагерцового излучения

возбуждением вытекающей моды плазменного слоя под действием пондеромоторных сил лазерного импульса

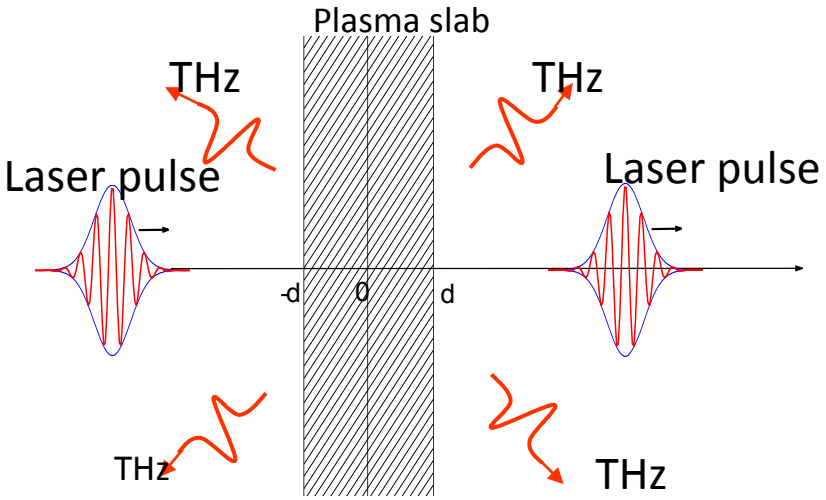

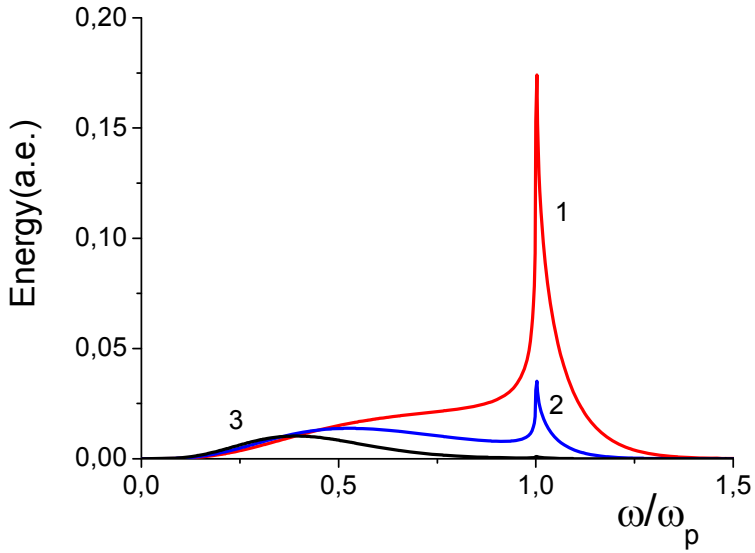

- ***Лазерный импульс:*** $\lambda_0 = 1\mu m$; $\tau = 50fs$ ($L = 15\mu m$); $R_L = 42\mu m$; $I_L = 4 \times 10^{17}\ W/cm^2$ ($W_L = 2J$; $P_L = 40TW$)
- ***Плазма:*** $2d = 120\mu m$; $N_{0e} = 1.3 \times 10^{17} cm^{-3}$
- ***ТГц излучение:*** $\nu_{THz} \approx 3.2\ THz$ ($\lambda_{THz} \approx 100\mu m$); $\tau \approx 0.8ps$; $W_{THz} \approx 0.8\mu J$; $P_{THz} \approx 1MW$; $W_{THz} / W_L \approx 8 \times 10^{-7}$

Спектр ТГц излучения в вакууме для различных длительностей лазерного импульса $(\omega_p \tau)^2 =$ 8,12, 20 при $(k_p R_L)^2 = 2$ и $k_p d = 1$.

$$W_{THz,\max} \simeq 0.1 \frac{\omega_p^2}{\omega_0^2} \frac{V_E^2}{4c^2} W_L$$

$$2d \simeq 2.4L$$

Фролов А.А. Генерация терагерцового излучения при падении лазерного импульса на слой разреженной плазмы // Физика плазмы. 2010. Т. 36. № 4. С. 347-364.

Исследование оптических и транспортных свойств в широком диапазоне параметров лазерной плазмы

Dielectric function in the relaxation time approximation

$$(-i\omega)\delta f + e\mathbf{E}\frac{\partial f_F(\mathbf{p})}{\partial \mathbf{p}} = -\nu_{ef}(p)\delta f$$

$$f_F(\mathbf{p}) = \frac{f_0(p)}{4\pi^3\hbar^3}$$

$$f_0(\mathbf{p}) = \left[1+\exp\left(\frac{\varepsilon(p)-\mu}{T_e}\right)\right]^{-1}$$

$$\varepsilon(\omega) = 1 + \frac{8\sqrt{2m_e}e^2}{3\pi\hbar^3\omega}\int_0^\infty \frac{\varepsilon^{3/2}d\varepsilon}{\omega + i\nu_{ef}(\varepsilon)}\frac{\partial f_0}{\partial \varepsilon}$$

$$\nu_{ef}(\varepsilon) = \min\left\{\sqrt{\frac{2\varepsilon}{m_e}}\frac{1}{r_0}, \frac{\varepsilon}{\pi\hbar}, \nu_C(\varepsilon), \nu_{met}(T_e, T_i, n_i)\right\}$$

$$\nu_C(\varepsilon) = \sqrt{\frac{2}{m_e}}\frac{\pi e^4 Z^2 n_i \Lambda(\varepsilon)}{\varepsilon^{3/2}}$$

Thermal and dc conductivities

•Boltzmann equation in linear approximation:

$$e\mathbf{E}\frac{\partial f_F(\mathbf{p},\mathbf{r})}{\partial \mathbf{p}}+\mathbf{v}\frac{\partial f_F(\mathbf{p},\mathbf{r})}{\partial \mathbf{r}}=-\nu_{ef}(p)\delta f$$

$$\mathbf{E}-\frac{1}{e}\nabla\mu=\frac{1}{\sigma}\mathbf{j}+\alpha\nabla T_e$$

$$\mathbf{q}'=\mathbf{q}-\left(\varphi+\frac{\mu}{e}\right)\mathbf{j}=\alpha T_e\mathbf{j}-\kappa\nabla T_e$$

•Kinetic coefficients:

$$\kappa=\frac{T_e^{5/2}}{3\pi^2\hbar^3}\sqrt{\frac{m_e}{2}}\left(I_{7/2}-\frac{I_{5/2}^2}{I_{3/2}}\right)$$

$$\sigma=\frac{e^2T_e^{3/2}}{3\pi^2\hbar^3}\sqrt{\frac{m_e}{2}}I_{3/2}$$

$$I_\beta(\eta)=\int_0^\infty\frac{x^\beta dx}{\nu_{ef}(x)}\,\mathrm{ch}^{-2}\left(\frac{x-\eta}{2}\right)$$

Transport properties

$$\nu = \min(\nu_{met}, \nu_{pl}, \nu_{max})$$

$$\nu_{met} = A_1 \frac{k_B T_i}{\hbar} + A_2 \frac{k_B T_e^2}{\hbar T_F}$$

on melting

$$\nu_{pl} = \frac{4\sqrt{2\pi} Z n_e m_e e^4}{3(m_e k_B T_e)^{3/2}}$$

$$\nu_{max} = \frac{\sqrt{v_F + k_B T_e / m_e}}{r_0}$$

$$\varepsilon = \varepsilon_{tb} + 1 - \frac{\omega_{pl}^2}{\omega_L(\omega_L + i\nu)} \frac{m}{m*}$$

$$\gamma_{ei} = A_3 \frac{3 m_e n_e \nu}{m_i}$$

$$\chi = A_4 \frac{k_B^2 n_e T_e}{m_e \nu}$$

$$R = \left| \frac{\sqrt{\varepsilon} - 1}{\sqrt{\varepsilon} + 1} \right|^2$$

	λ_L, mkm	n	k	$\varepsilon_1 = n^2 - k^2$	$\varepsilon_2 = 2nk$	R
Cu	0.83	0.260	5.26	-27.60	2.74	0.964
Cu	1.24	0.433	8.46	-71.38	7.33	0.976
Au	0.83	0.188	5.39	-29.02	2.03	0.975
Au	1.24	0.372	8.77	-76.77	6.52	0.981

Handbook of optical constants of solids, E. Palik *et al.*

Wide range approximations of transport properties

Dielectric function

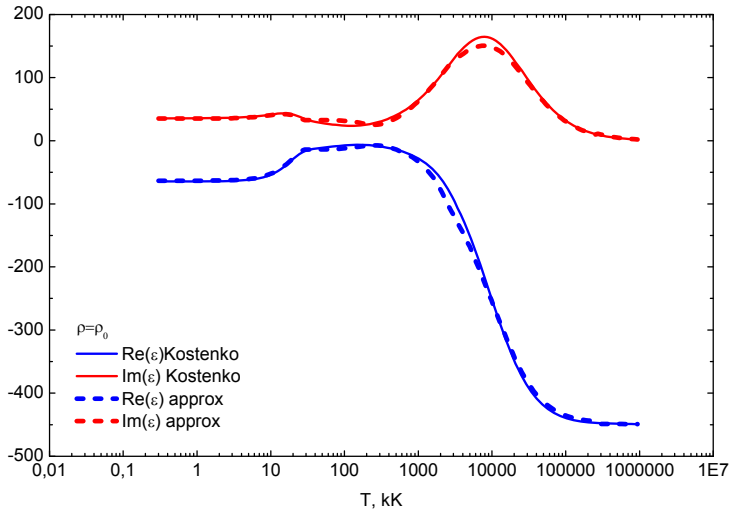

Thermal conductivity

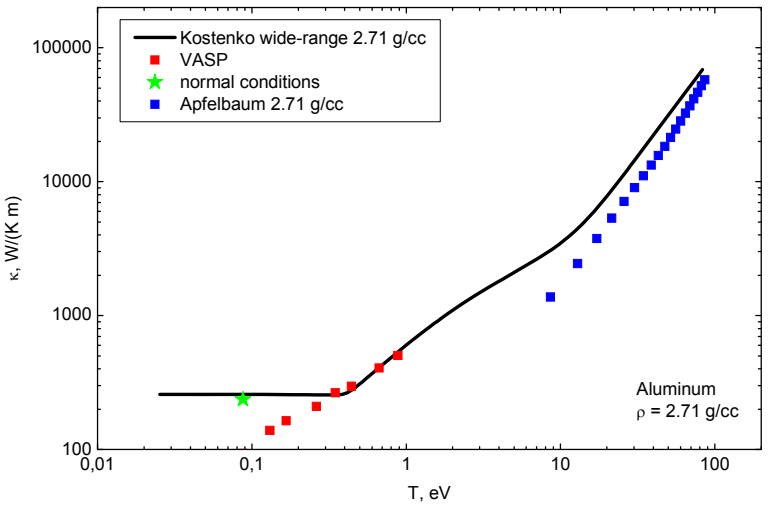

In the experiment the bulk aluminum target was heated by normal incident laser pulse with intensity 10^{14} W/cm^2, laser wavelength 400 nm and full width at half maximum (FWHM) 120 fs. Two probe pulses with FWHM 110 fs, 800 nm wavelength and angle of incidence 45◦ were used

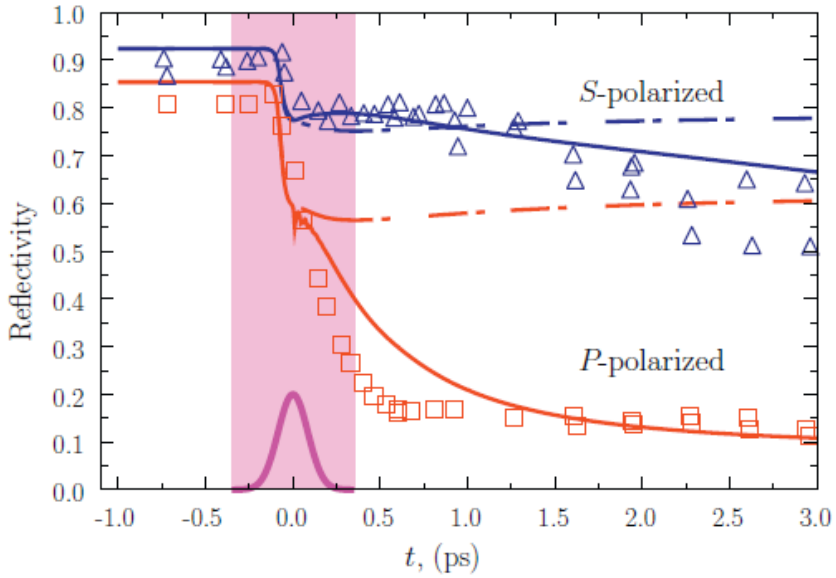

Experimental reflectivity dynamics for the S- (blue triangles) and the P-polarized (red squares) probe pulses. Corresponding simulation results are pre-sented by the blue and red solid lines, respectively. Dash-and-dot lines show the reflectivity changes for "frozen motion" regime.

K. Widmann, et al., Phys. Plasmas 8 (2001) 3869–3872.

Mikhail E. Povarnitsyna,∗, Nikolay E. Andreeva,b, Eugeny M. Apfelbauma, Tatiana E. Itina a,c, Konstatntin V. Khishchenkoa,b, Oleg F. Kostenkoa, Pavel R. Levashova,b, Mikhail E. Veysmana Applied Surface Science *xxx (2011) xxx– xxx*

Создание широкодиапазонных моделей термодинамических свойств плотного горячего вещества с учетом возбуждения электронов внутренних электронных оболочек

Работа выполняется в сотрудничестве с Лабораторией № 1.7.1 (31) ОИВТ РАН – широкодиапазонных уравнений состояния

Учет зависимости плотности электронных состояний от температуры важен для описания термодинамических свойств вещества аналитическими моделями

Плотность электронных состояний для **твердотельного алюминия:** зависимость от температуры существенна!

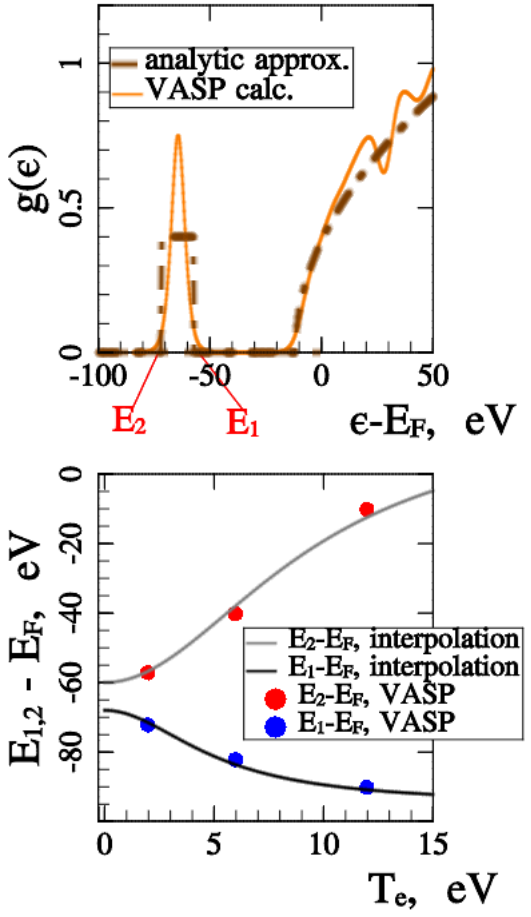

Зависимость давления и теплоемкости от температуры для **твердотельного алюминия**

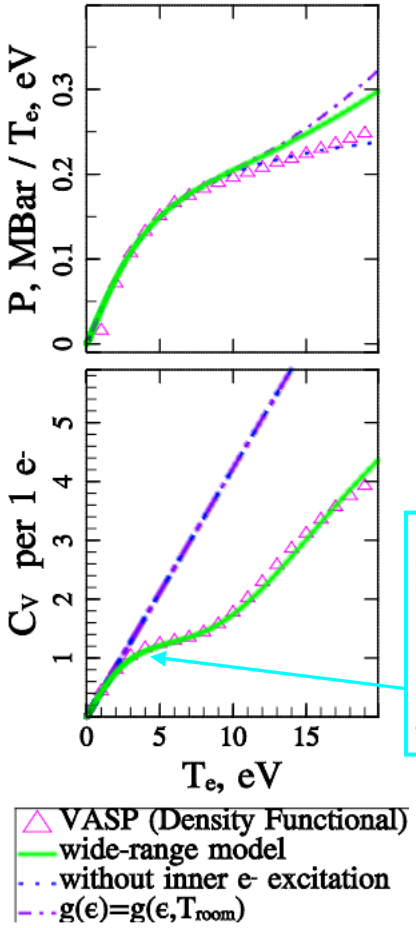

Возбуждение P-оболочки из-за модификации g(ε) при возрастании температуры

Зависимость давления и удельной внутренней энергии от температуры для **твердотельного серебра**

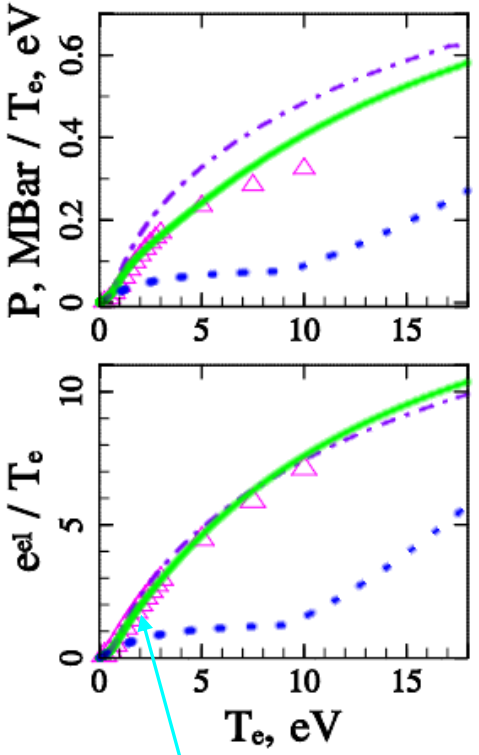

Возбуждение d-оболочки из-за близости к E_F

Аналитическая модель с приближенной плотностью состояний, как показывает сравнение с VASP-расчетами, правильно передает вклад возбуждения d или p -электронов в удельную энергию и давление электронной компоненты простых и благородных металлов

Разработанная широкодиапазонная кинетическая модель диэлектрической проницаемости ε находится в хорошем согласии с данными квантово - статистических расчетов по методу линейного отклика в области высоких температур

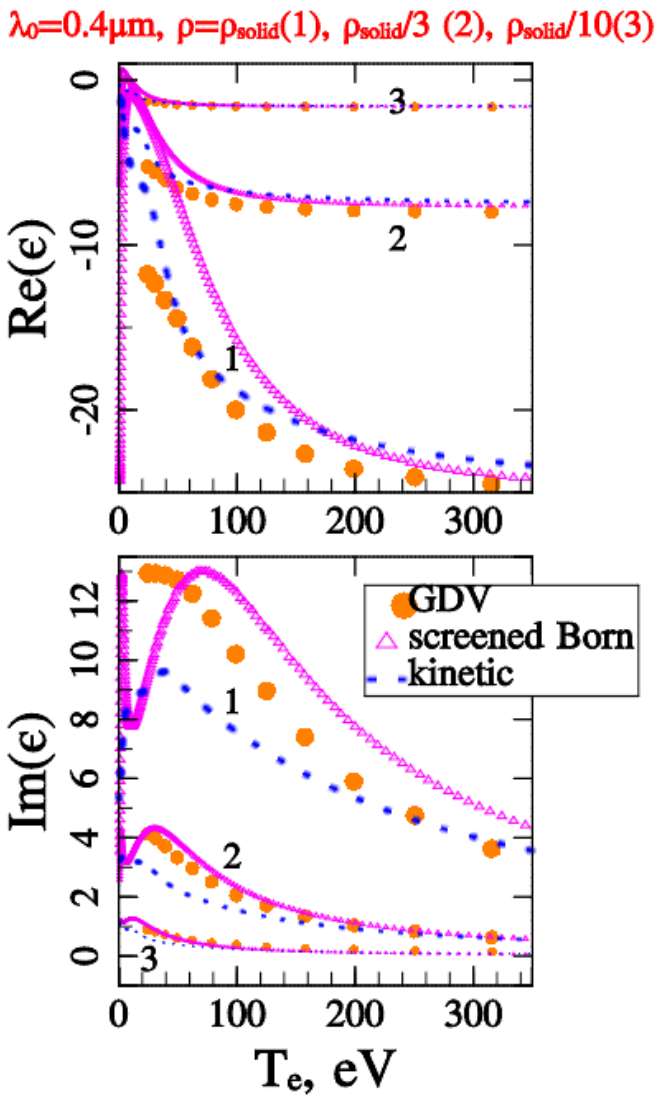

При температурах < 100 эВ отличие кинетической модели от квантово-статистических расчетов связаны с учетом **поляризационных эффектов** (**экранированное Борновское приближение**) и **сильных столкновений** с рассеянием на большие углы (**приближение**

$$\varepsilon_{sc}^{\mathrm{B}}(\omega) = 1 - \frac{n_e}{n_c}\frac{1}{1 + i\nu_{sc}^{\mathrm{B}}(\omega)/\omega} \qquad \nu_0 = \frac{2Z}{3\pi}\sqrt{\frac{Rd}{T_e}}$$

$$\nu_{sc}^{\mathrm{B}}(\omega) = -i\nu_0 \int_0^{\infty} \frac{k^2 dk}{[1+\omega_p^2/k^2]^2} \frac{\varepsilon_{RPA}(k,\omega) - \varepsilon_{RPA}(k,0)}{\omega}$$

$$\varepsilon_{kin}(\omega) = 1 - \frac{n_e}{n_c}\frac{\epsilon_F^{-3/2}}{m_{\mathrm{opt}}} \int_0^{\infty} \frac{e^{\xi-\epsilon_\mu}\xi^3 d\xi}{\left[1+e^{\xi-\epsilon_\mu}\right]^2} \frac{\xi^{3/2} - i\nu_T(\omega)}{\xi^3 + \nu_T^2(\omega)}$$

$$\nu_T(\omega) = \frac{\nu_{\mathrm{eff}}}{\omega}\epsilon_F^{3/2}\left[1 + e^{-\epsilon_\mu}\right]$$

При оптических частотах и высоких температурах широкодиапазонная кинетическая модель ε хорошо согласуется с квантово-статистической моделью.

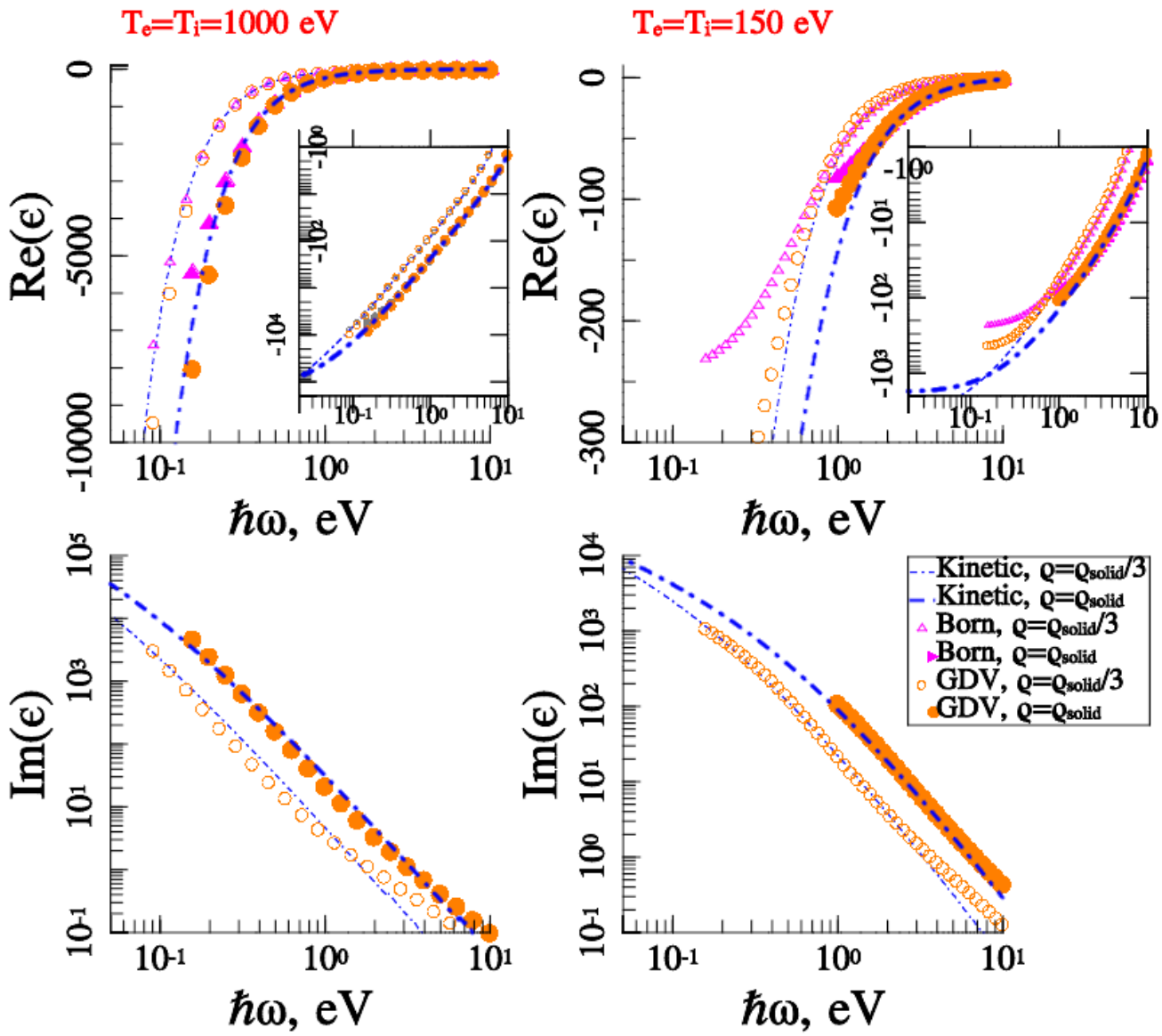

При низких частотах квантово-статистическая одномоментная модель занижает мнимую часть ε и завышает действительную часть ε .

Требуется учет более высоких моментов функции распределения в квантово-статистической модели

Femtosecond Laser System at JIHT

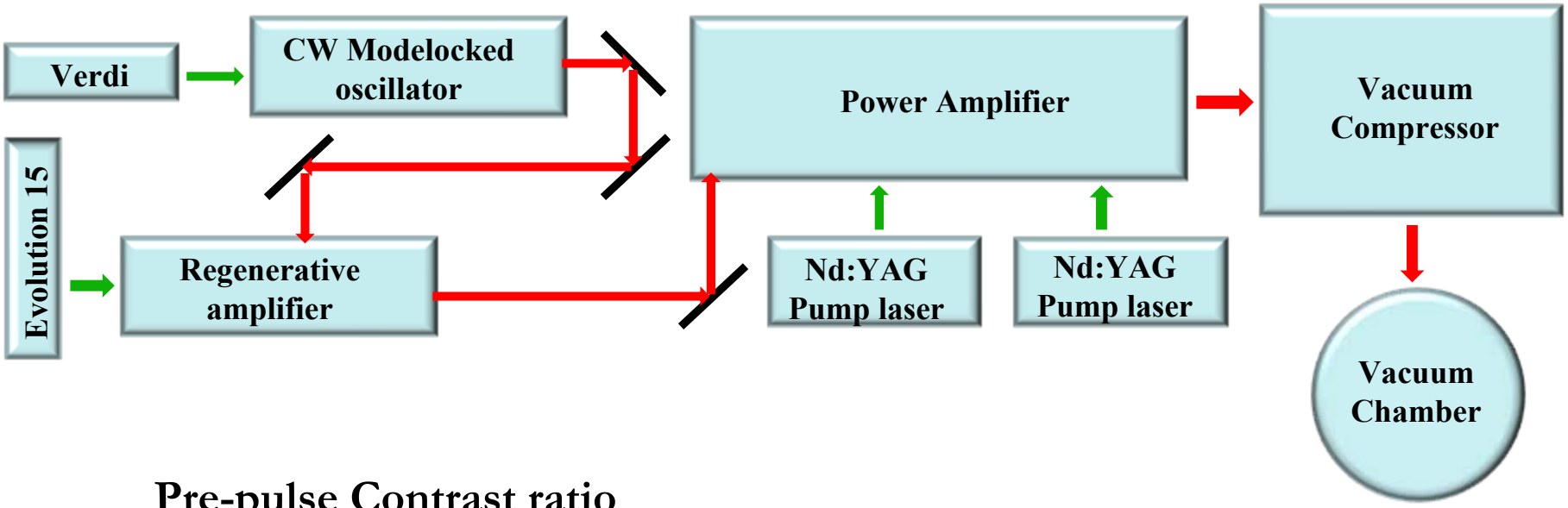

Pre-pulse Contrast ratio

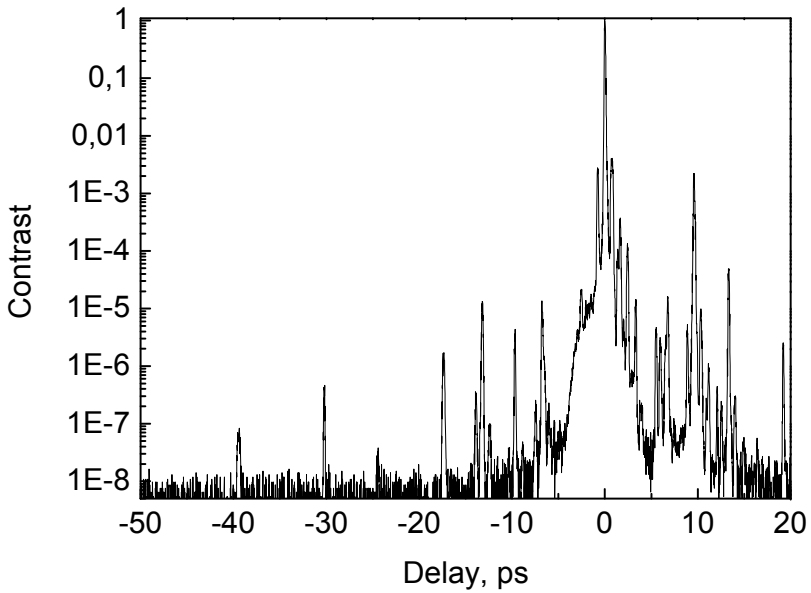

Laser parameters	
Center wavelength, nm	~ 800
Pulse duration (FWHM), fs	37 ± 5
Output energy	> 250 mJ
M^2 Figures	$M^2_x = 1.5$ $M^2_y = 1.35$
Bandwidth (nm)	~ 28 nm
Beam diameter ($1/e^2$)	30 mm

WDM collaboration – Atomic physics in dense environments

WDM produced by Intense Heavy Ion Beams and probed by Intense Laser Beams

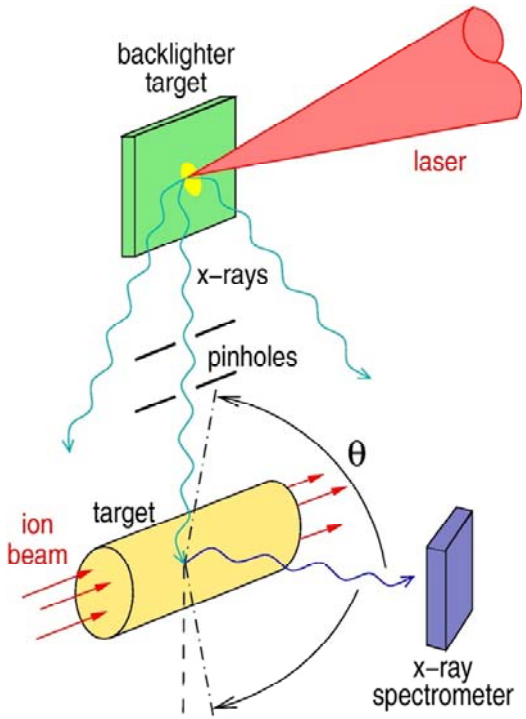

Unique combination of intense heavy ion beam driven experiments + PHELIX driven diagnostics

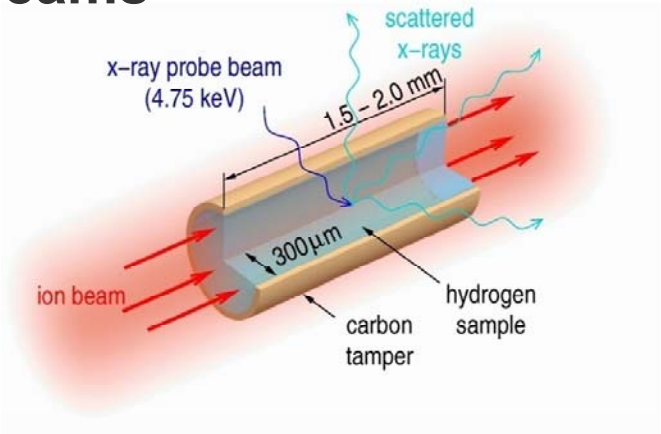

High Power Laser PHELIX

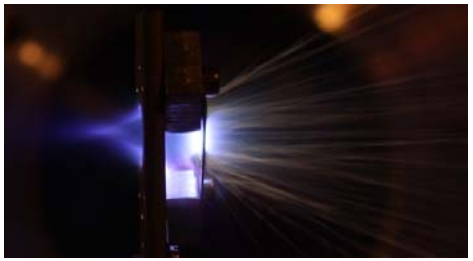

PHELIX prepulse reduction by the foil in front of the X-ray target

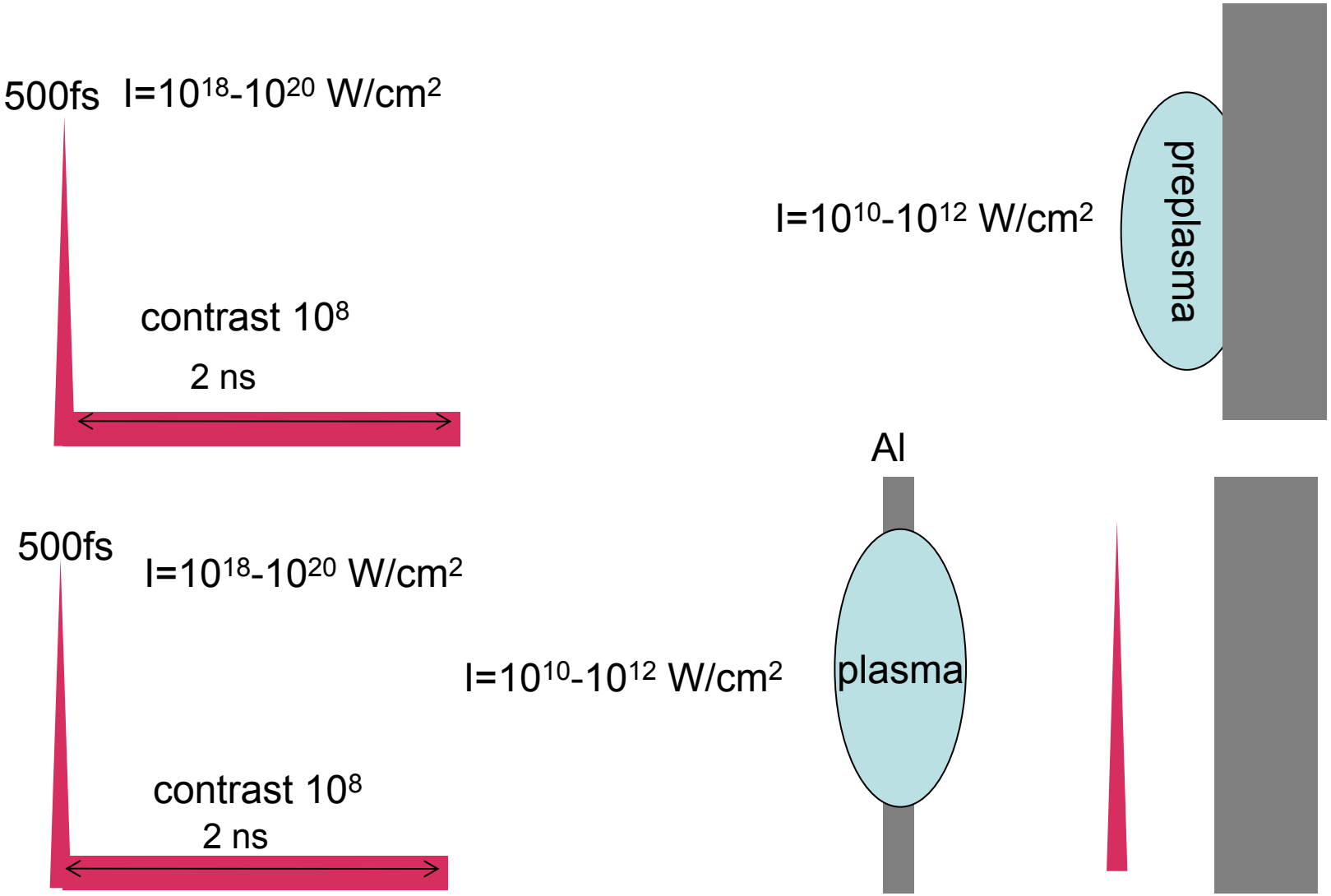

Динамика предимпульса, защитной фольги и мишени

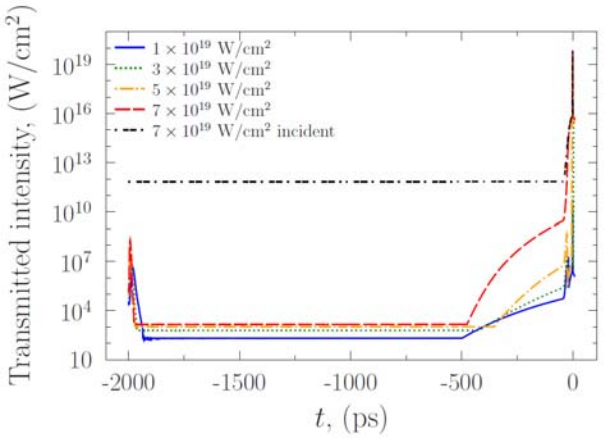

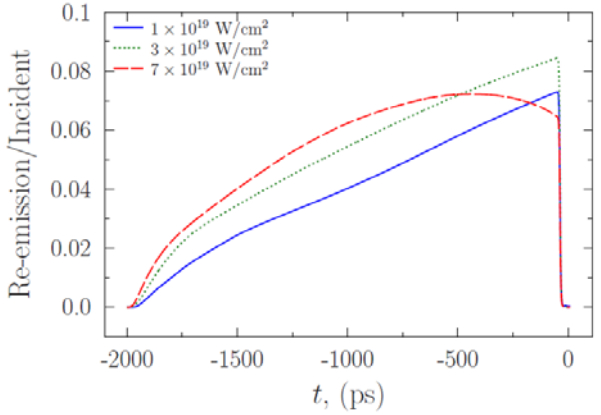

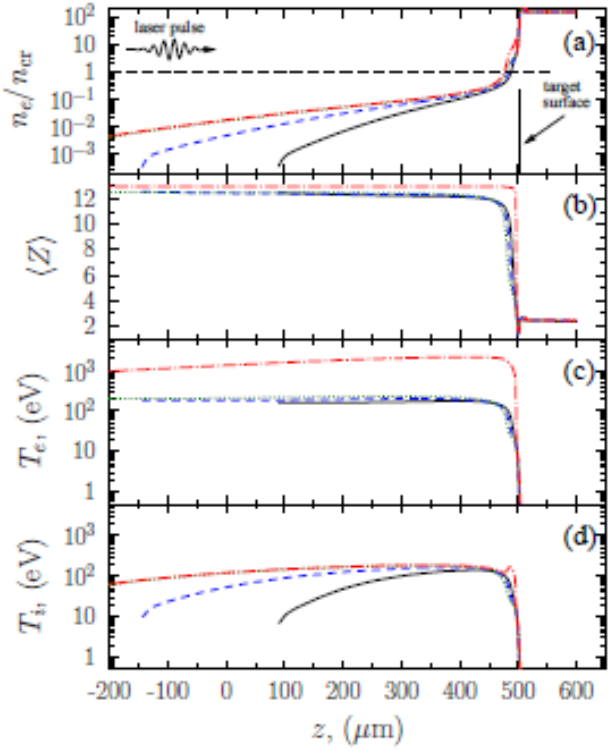

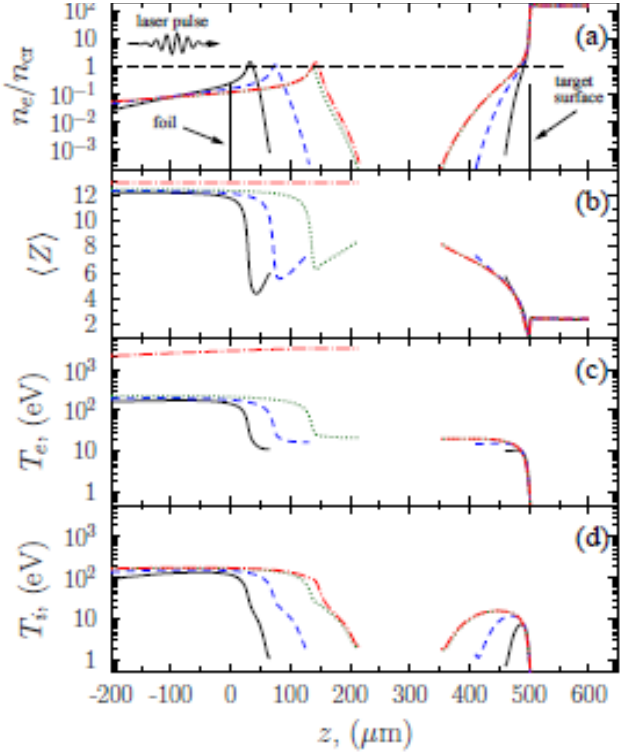

Laser Acceleration:

At $10^{23} W/cm^2$, E= 0.6PV/m,
it is SLAC (50GeV, 3km long) on 10μm
The size of the Fermi accelerator will only be one meter (PeV accelerator that will go around the globe, based on conventional technology).

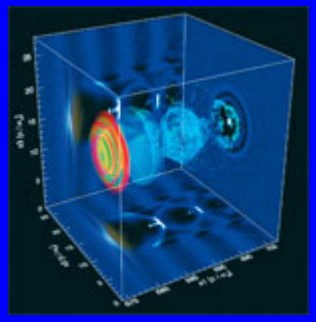

Exponential growth of "the Livingston curve" began tapering off around 1980

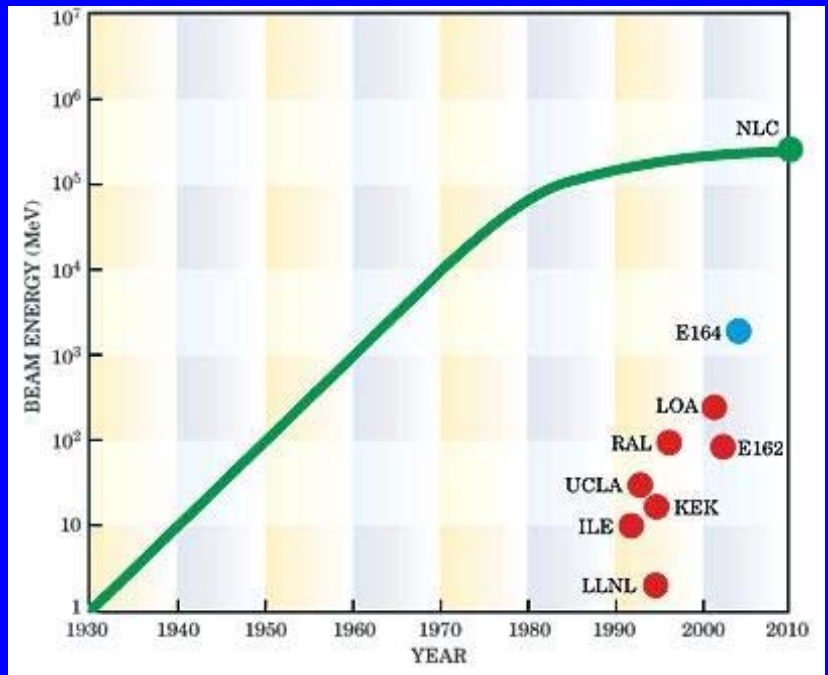

IHED
JIHT RAS

Expected potential
of laser – plasma acceleration of electrons

Electric field of plasma wave (*with phase velocity ~ c, $\lambda_p = 2\pi c/\omega_p$*):

$$E_P\,[V/m] \approx 10^2\,\alpha\;(\,n_e\,[cm^3]\,)^{1/2} \propto \gamma_g^{-1} = \omega_p/\omega_0$$

$\alpha = \delta n / n_0$ – plasma wave amplitude; at α = 0.3÷1.0, $n_e = 10^{17} \div 10^{18}$ cm^{-3}:

$$E_P = 10 \div 100\ GV/m$$

maximum of accelerating gradient in traditional accelerators (RF linac):

$E_{RF} \sim 10 - 100$ MV/m

Exponential growth of "the Livingston curve" began tapering off around 1980

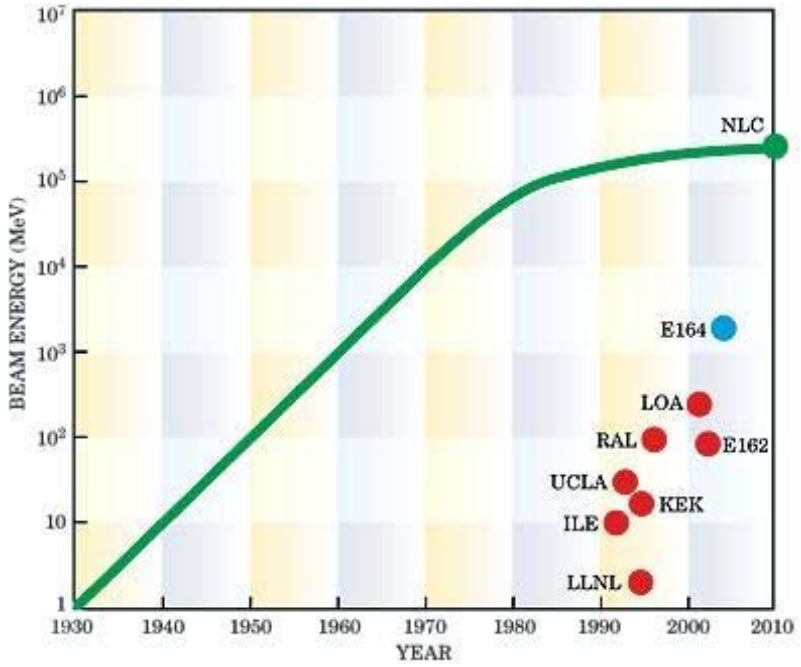

Electron-Positron Linear Collider

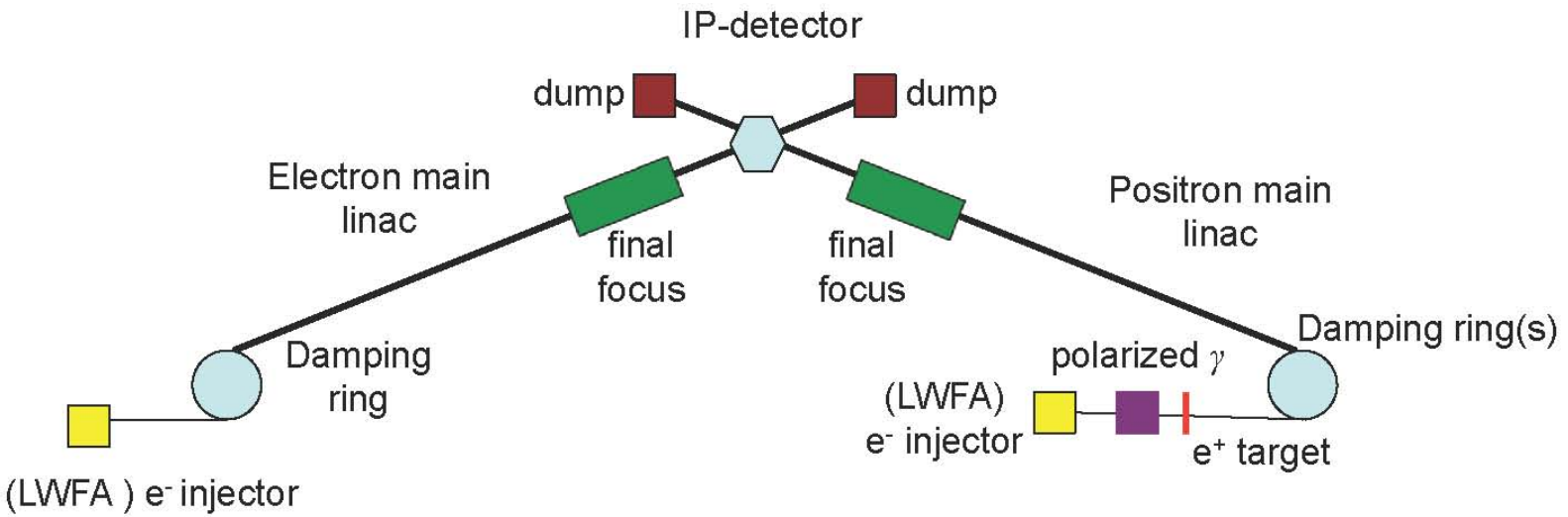

Conventional technology:

- Current generation of future linear collider designs based on existing technology (e.g., ILC): E_{cm}~ 0.5 TeV; gradient ~ 0.03 GV/m; ~30 km (~multi-$B).
- Higher energy collider with existing technology: 5 TeV ➔ >100 km, > tens of $B

Laser plasma accelerator based concept for a Laser Plasma Linear Collider

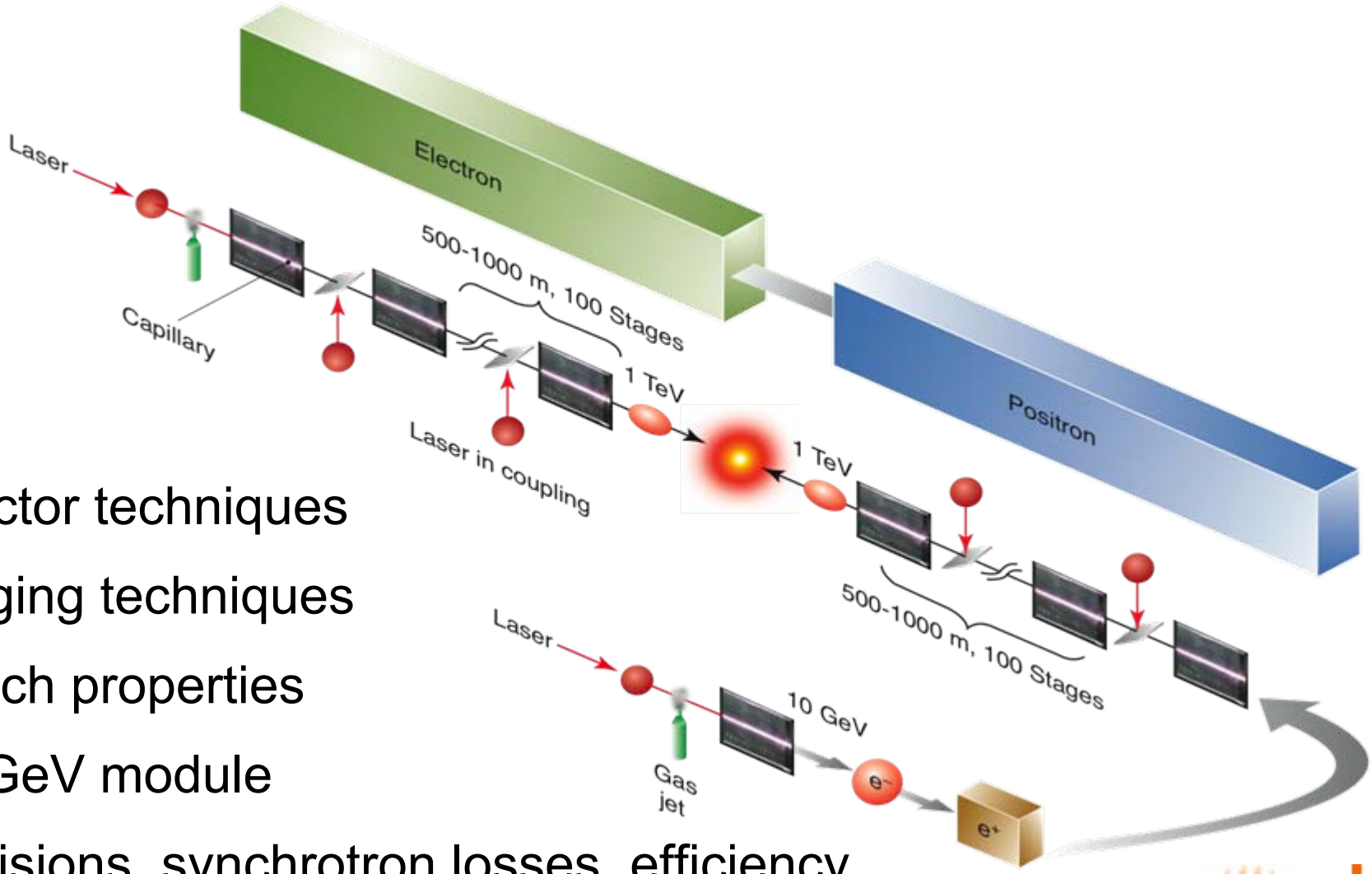

- Injector techniques
- Staging techniques
- Bunch properties
- 10 GeV module
- Collisions, synchrotron losses, efficiency

C.B. Schroeder et al., AAC Proceedings 2008: Leemans & Esarey, Physics Today, March 2009

Parameters and results of some experiments

for **standard LWFA** scheme $c\tau_L \approx \lambda_p/2$

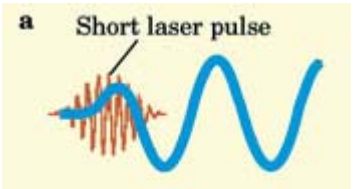

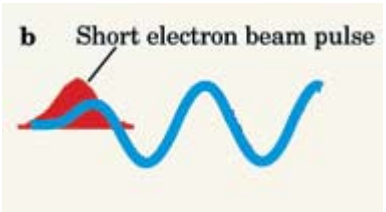

Tunable monoenergetic bunches

Z_{inj}=225 μm

Z_{inj}=-75 μm

Z_{inj}=-275 μm

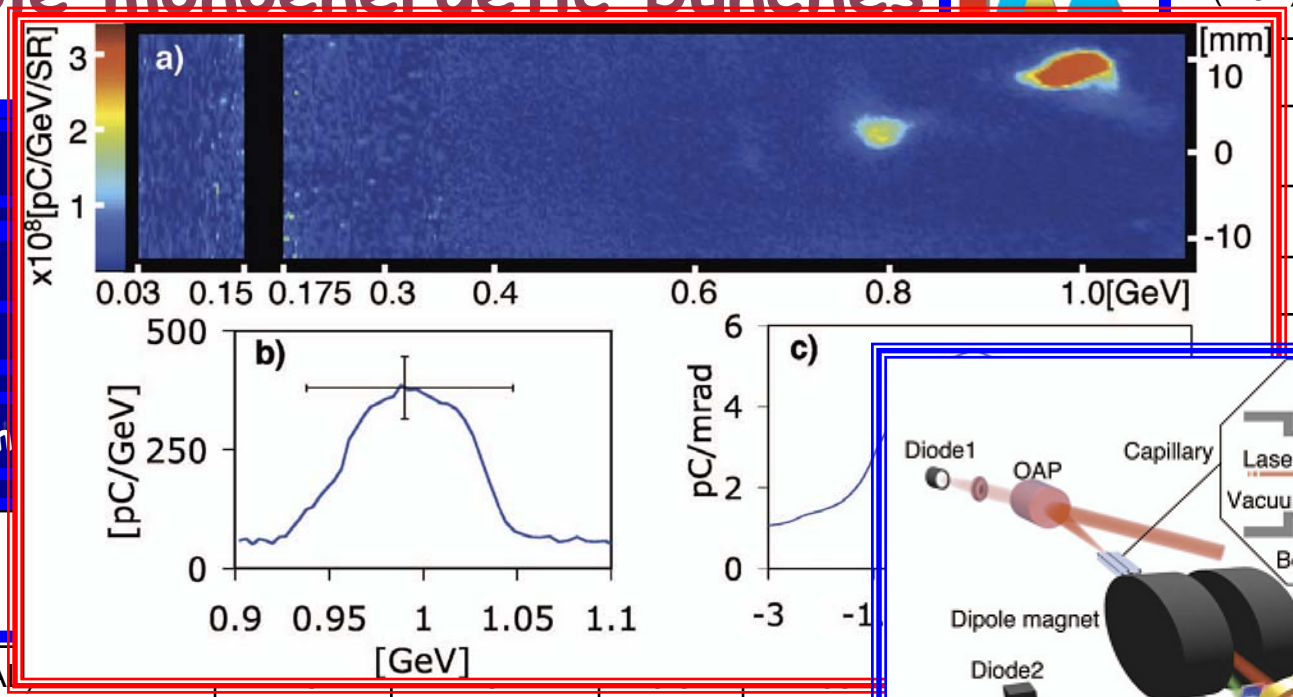

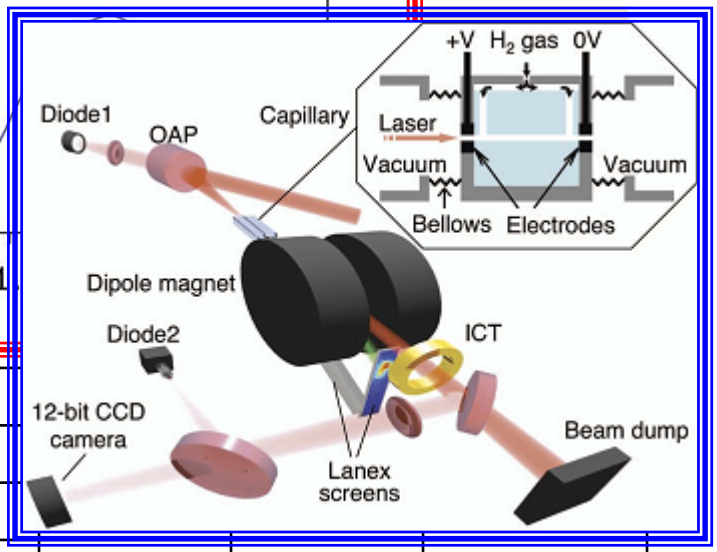

					ΔE (MeV)		E_{ac} (GV/m)
UK (RA							0.7
France (CEA)	5	10^{19}	0.3	1.05			1.5
USA (CUOS)	4.5	10^{18}	0.4	1.05			20
USA (NRL)	2.5	4×10^{18}	0.4	1.05			**200**
Japan (KEK)	3	10^{17}	1.0	1.05	10^{19}	17	30

Scheme of one cascade of the laser wake-field accelerator

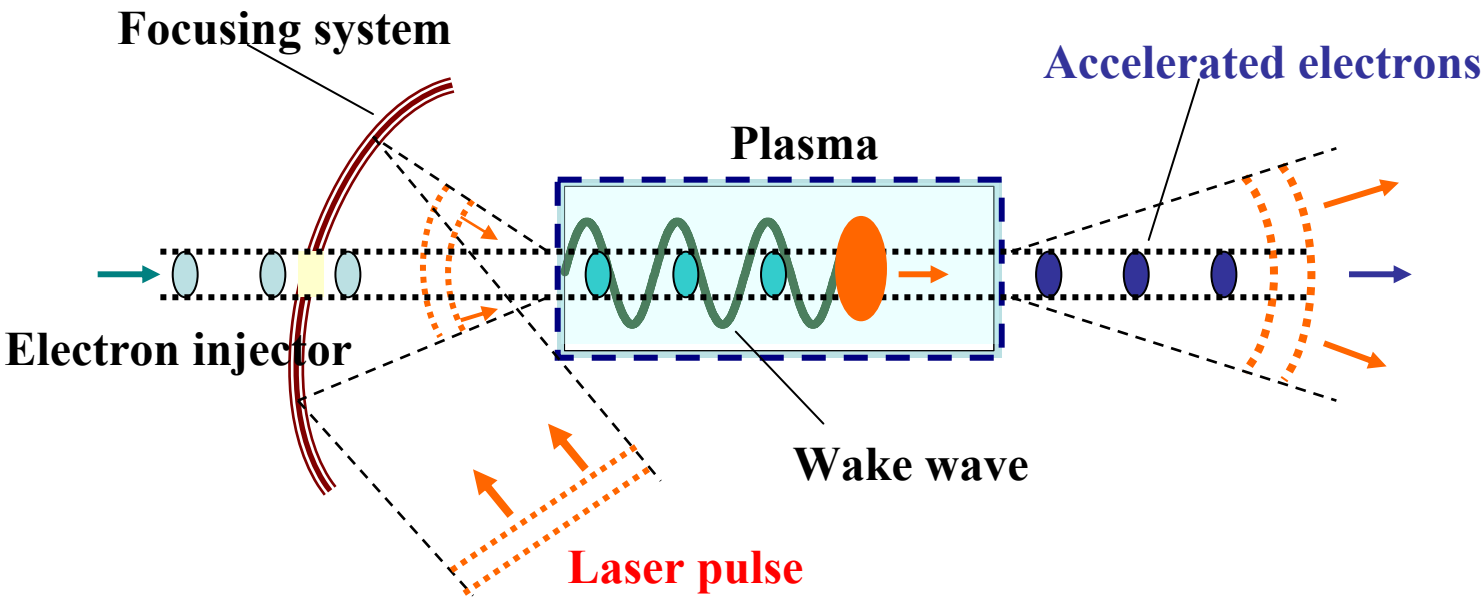

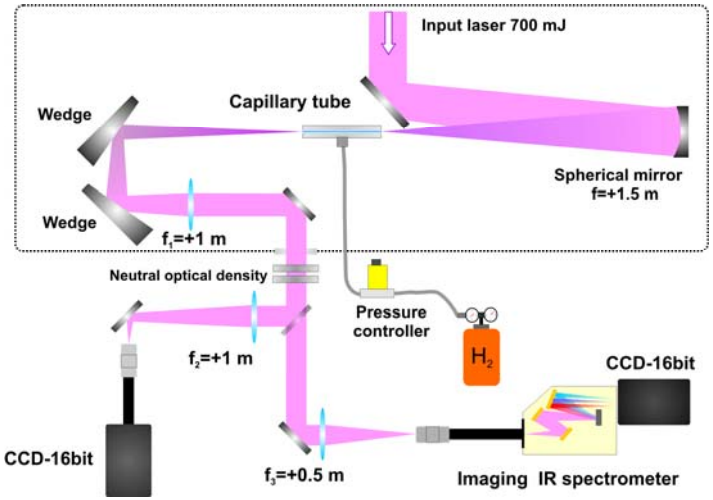

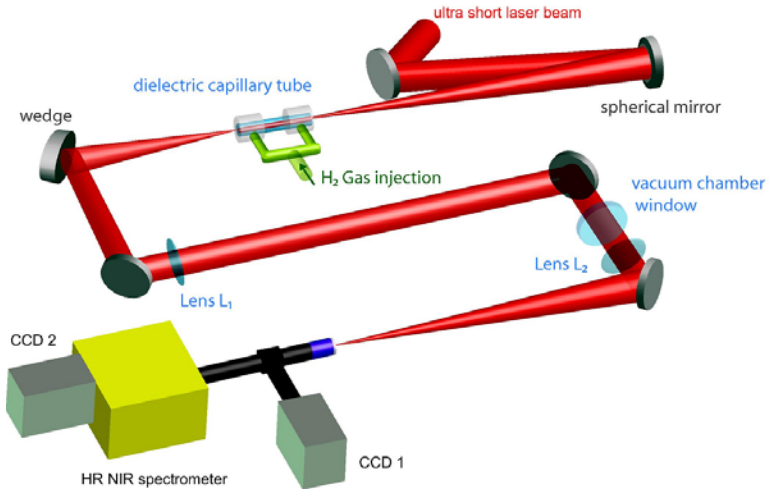

B. Cros, et al. Schematic view of the experiment **at the Lund Laser Center**

Physical Restrictions on the Energy of Accelerated Electrons in Laser-Plasma Accelerators

Maximum length of acceleration:

$$l_{acc} \le L_{deph} = \frac{\lambda_p}{2(c - v_{ph})} c = \gamma_g^2 \lambda_p, \qquad \gamma_g = \frac{\omega_0}{\omega_p} = \sqrt{\frac{n_c}{n_e}}$$

Phase velocity: $V_{ph} \simeq V_g = \partial\omega / \partial k = c\sqrt{1 - \omega_p^2 / \omega^2}$ $\quad \gamma_g = 1/\sqrt{1 - V_g^2 / c^2}$

$$k^2 c^2 = \omega^2 \varepsilon(\omega) = \omega^2 - \omega_p^2; \quad \varepsilon = 1 - \omega_p^2 / \omega^2 \equiv 1 - n_e / n_{cr}$$

E_P [V/m] ≈ 10^2 α (n_e [cm^3])$^{1/2}$ $\qquad \propto \gamma_g^{-1} = \omega_p / \omega_0$

Energy gain: $\Delta W_e = eE_a l_a \cong \frac{e\Delta\varphi}{\lambda_p / 2} l_a = 2mc^2 \gamma_g^2 \alpha$

for 1 μm laser: at γ_g~100 & α~1, ΔW_e~ 10 GeV and L_{deph}= 1 m

Wakefield generation by guided laser pulses

➢ *spectroscopic diagnostics of the wakefield*

$$\tilde{E}(r) = \sum_{n=1}^{N_m} C_n J_0(k_{\perp n} r), \quad k_{\perp n} = \frac{u_n}{a} - i\frac{u_s}{k_{w\perp} a^2}$$

$$C_n = \frac{2}{[a\,J_1(u_n)]^2} \int_0^a E(r) J_0(u_n r / a)\, r dr, \quad J_0(u_n) = 0$$

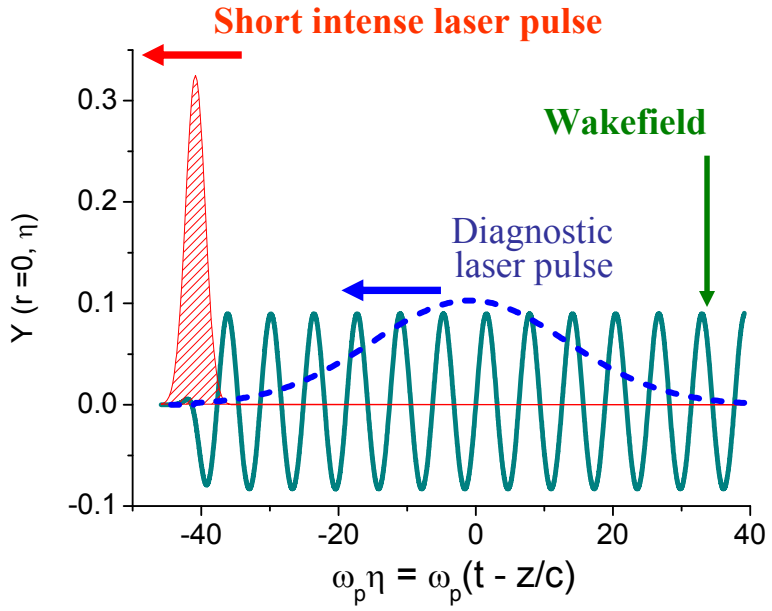

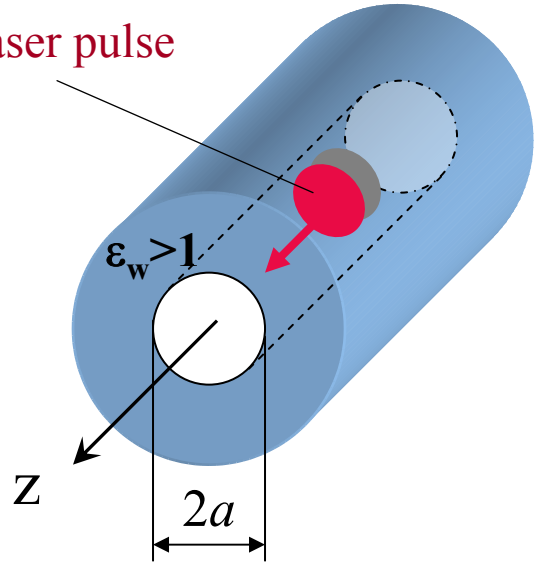

Laser energy leakage:

$$I_L(z) = I_0 \exp(-z / L_D)$$

$$L_{D,n}^{-1} = \frac{u_n^2}{k_0^2 a^3} \frac{1+\varepsilon_w}{\sqrt{\varepsilon_w - 1}}$$

Spectral diagnostics of the laser wake fields in capillary tubes

The average product of gradient and length achieved in this experiment is of the order of 0.4 GV at a pressure of 50 mbar @ 0.12 J, 51 fs

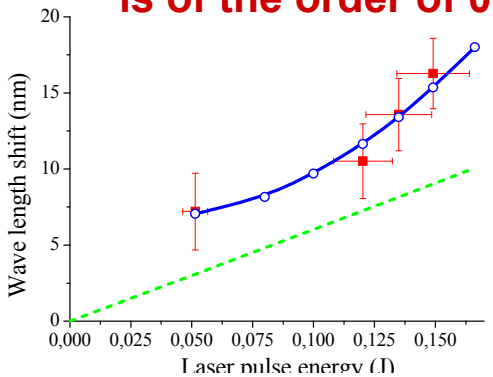

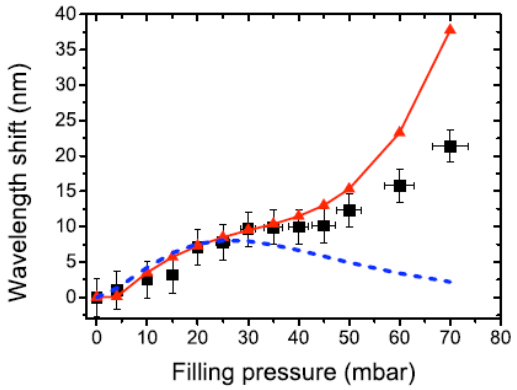

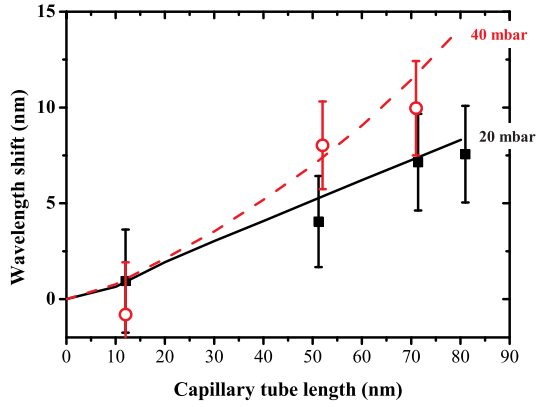

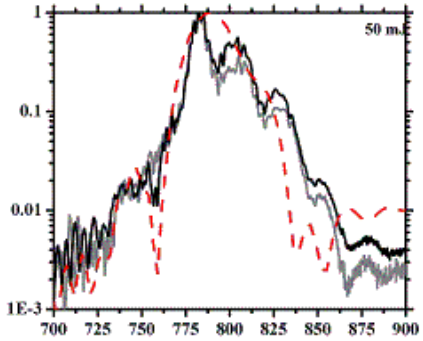

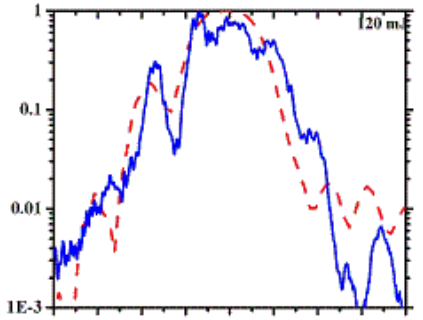

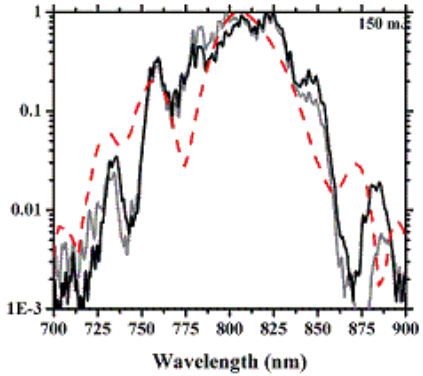

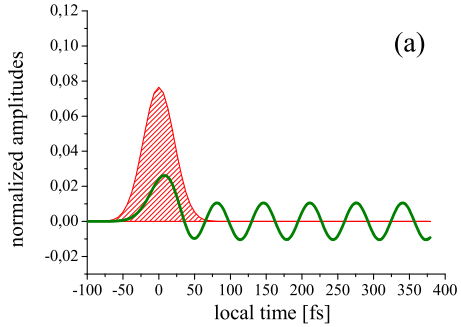

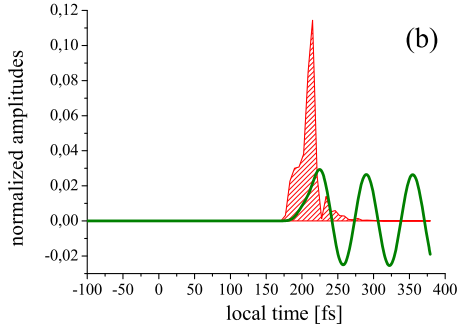

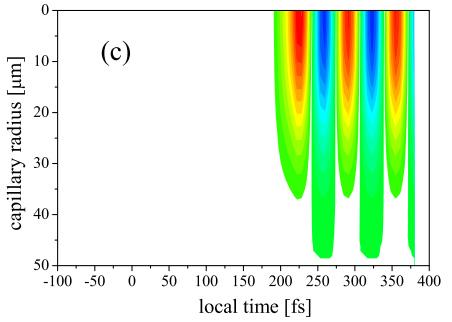

N.E. Andreev, et al, NJP, v. 12, 045024 (2010)

Energy spread in LWFA of short e-bunches

Electron bunch injection into LWFA at the maximum of accelerating field

Parameters of the laser pulse and electron bunch

$$a_0 = \frac{|e|E_L}{mc\omega} = 1.0 \qquad \gamma_{ph} = \omega/\omega_p = 50 \qquad E_{inj} = 80\, mc^2 \qquad \mathbf{L_b = 0.1 k_p^{-1}}$$

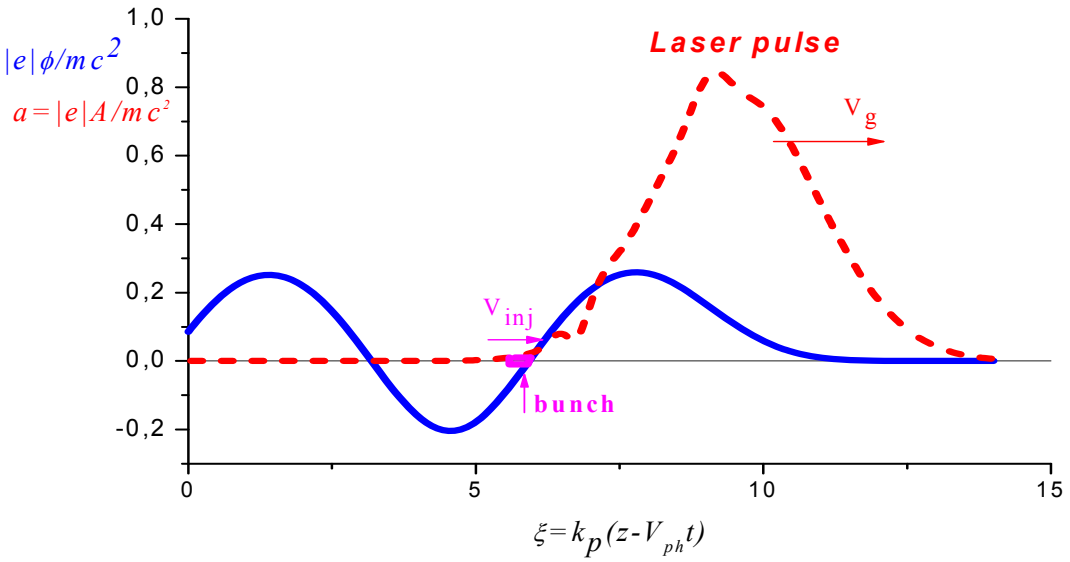

$$E_{\max} \approx 2mc^2\gamma_{ph}^2\,\varphi_{\max}$$

$$|\Delta E| \approx 2mc^2\gamma_{ph}^2 k_p L_{b0}\left\{\frac{d\phi(\xi_{inj})}{d\xi}\right\}$$

without loading effect

$$\Delta E / E_{\max} \simeq k_p L_b \simeq 10\%$$

for $L_b \approx$ 1mkm (3fs !)

Electron Bunch Injection in Front of the Laser Pulse

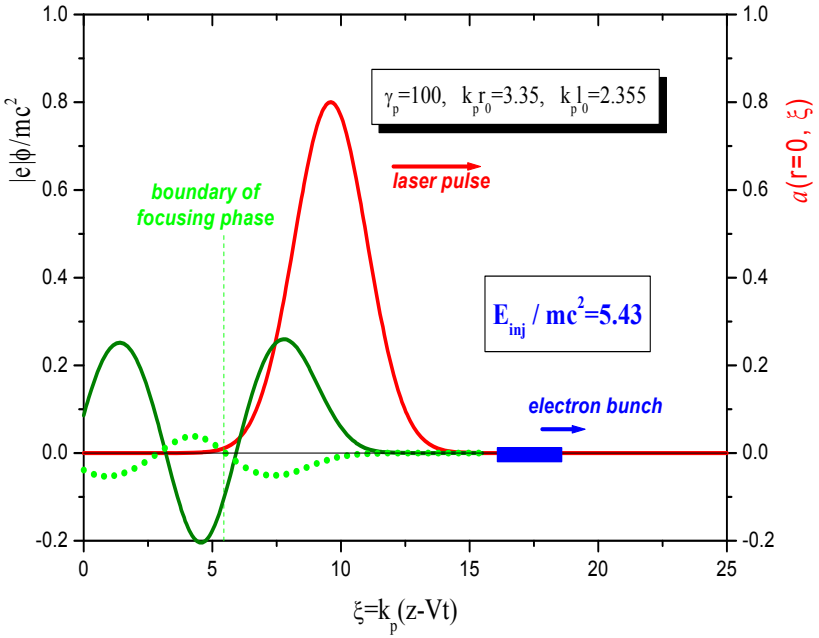

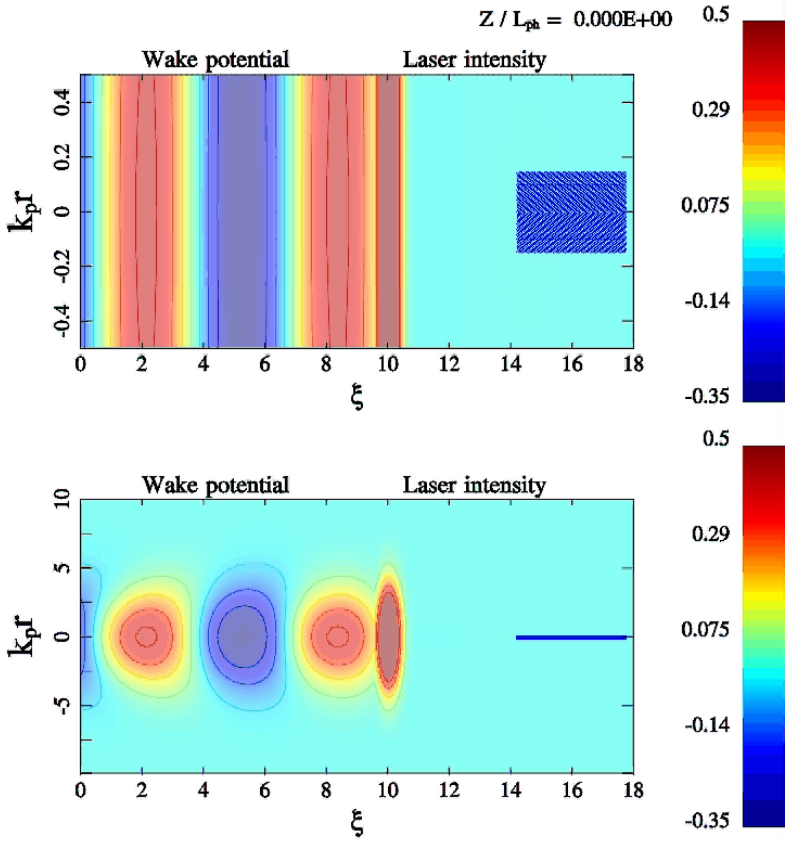

For the velocity of injected electrons

$$u_{inj} = c\sqrt{1 - m^2c^4 / E_{inj}^2} < v_{ph} \quad :$$

$$\frac{\Delta E}{mc^2} = 2\gamma_{ph}^2 k_p L_b \left\{ \left(\frac{d\varphi}{d\xi_{inj}} - \frac{d\varphi}{d\xi} \right) + \frac{k_p L_b}{2} \left(\frac{d^2\varphi}{d\xi^2} - \frac{d^2\varphi}{d\xi_{inj}^2} \right) \right\}$$

$$\frac{L_b}{L_{b0}} = \frac{1-\beta}{\beta - u_{inj}/c} \qquad \beta = v_{ph}/c$$

Long low-energy electron bunch will be trapped and compressed in the wakefield

N.E Andreev., S.V. Kuznezov. Electron Bunch Compression in Laser Wakefield Acceleration.// http://www.nuclear.jp/~icfa/GIENS/workshop_papers/giens01.pdf: *Giens Workshop Proceedings, June 24 - 29, 2001.*

Electron Bunch Injection in Front of the Laser Pulse

trapping and compression

bunch injected in front of the laser pulse can be trapped and compressed in the wake field, if the condition

$$-\varphi(\xi_{tr}) = E_{inj}/mc^2 - \left[\left(1-\gamma_{ph}^{-2}\right)\left(E_{inj}^2/m^2c^4-1\right)\right]^{1/2} - 1/\gamma_{ph}$$

is fulfilled in the focusing phase of the wakefield

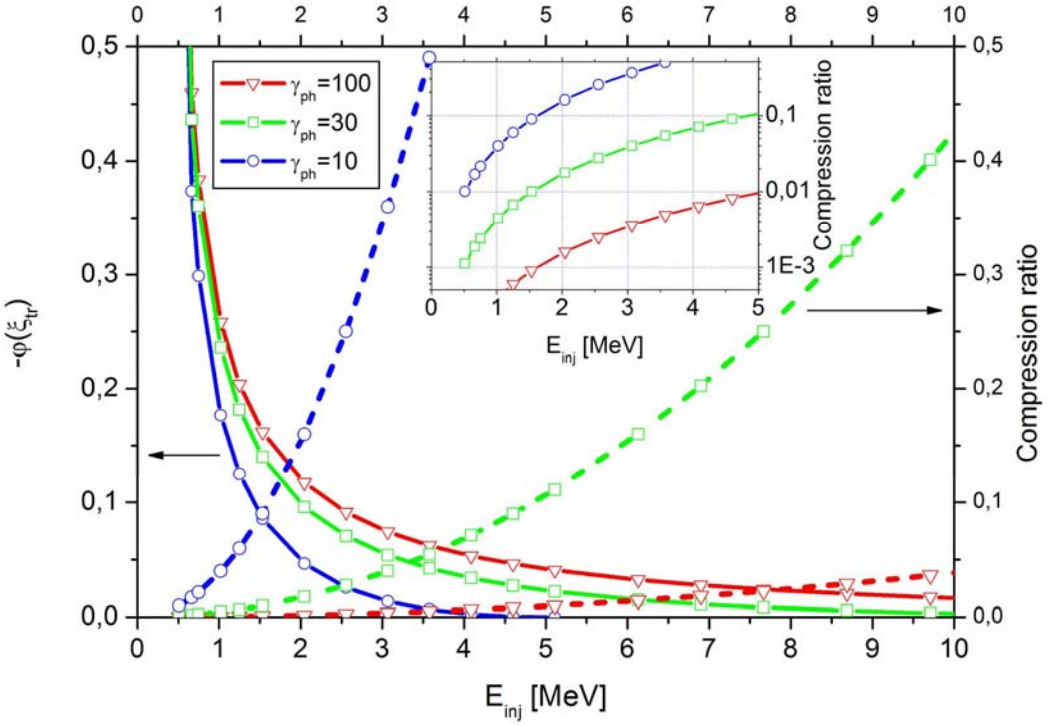

$$\frac{L_{b,rms}}{L_{b0}} \cong \frac{c-V_{ph}}{V_{ph}-u_{inj}} \approx \frac{E_{inj}^2}{\gamma_{ph}^2 m^2 c^4}$$

N.E. Andreev, S.V. Kuznetsov, et al, Plasma Phys. Control. Fusion, 52 (2010)

Electron Bunch Injection in Front of the Laser Pulse

energy spread at the end of acceleration

$$E_{\max} \cong 2\gamma_{ph}^2 mc^2 \varphi_{\max}$$

$$\frac{\Delta E_{\min}}{E_{\max}} \cong \frac{1}{2}(k_p L_{b,rms})^2 \cong 2\pi^2 \gamma_{ph}^{-6} \left(\frac{E_{inj}}{mc^2}\right)^4 (L_{b0}/\lambda_0)^2$$

$$\frac{\Delta E_{\min}}{mc^2} = \gamma_{ph}^2 (k_p L_{b,rms})^2 \left|\frac{d^2\varphi}{d\xi_{\max}^2}\right|$$

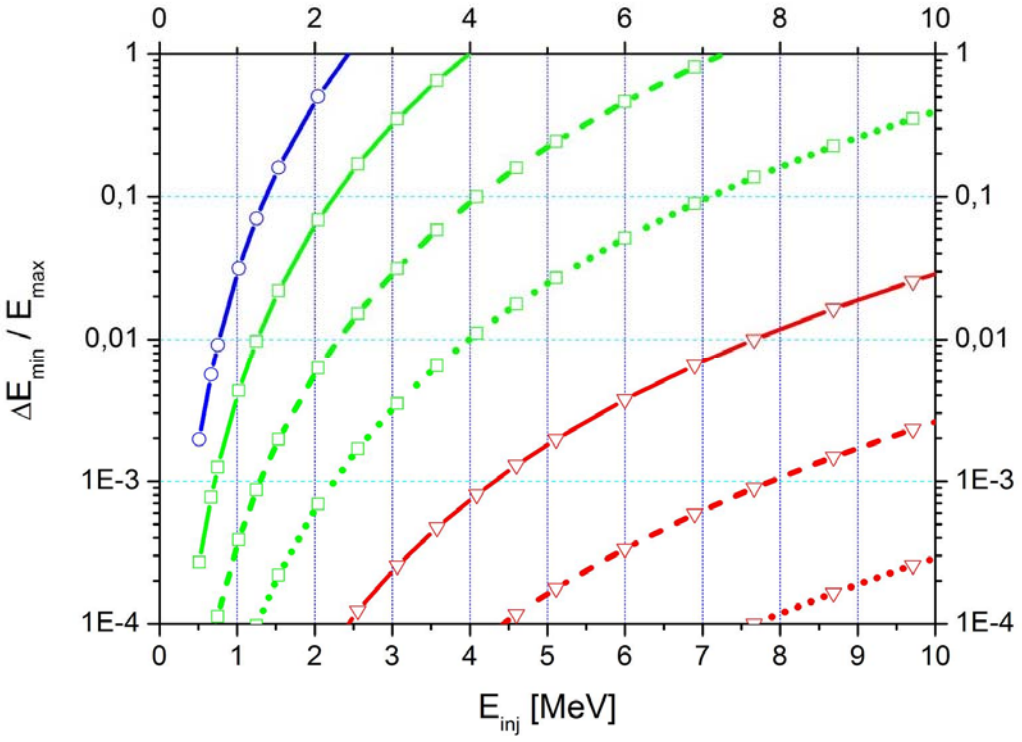

$\gamma_{ph} = 100$, 30, and 10 marked by triangles, squares and circles respectively, and for three initial bunch lengths $L_{b0} = 100$, 30, and 10 μm (solid, dashed and dotted lines respectively) for the laser wave length $\lambda_0 = 1$ μm

Динамика в фазовом пространстве
немоноэнергетического сгустка конечной длины,
ускоряемого кильватерной волной.

$$\left|\Delta E(\xi_f)\right| = 2\gamma_{ph}^2 |e| \cdot \frac{d\phi}{d\xi_f} k_p L_b(\xi_f) \approx 2|e| \cdot \frac{d\phi}{d\xi_{tr}} \frac{E_{inj}^2}{m^2 c^4} k_p L_{b0}$$

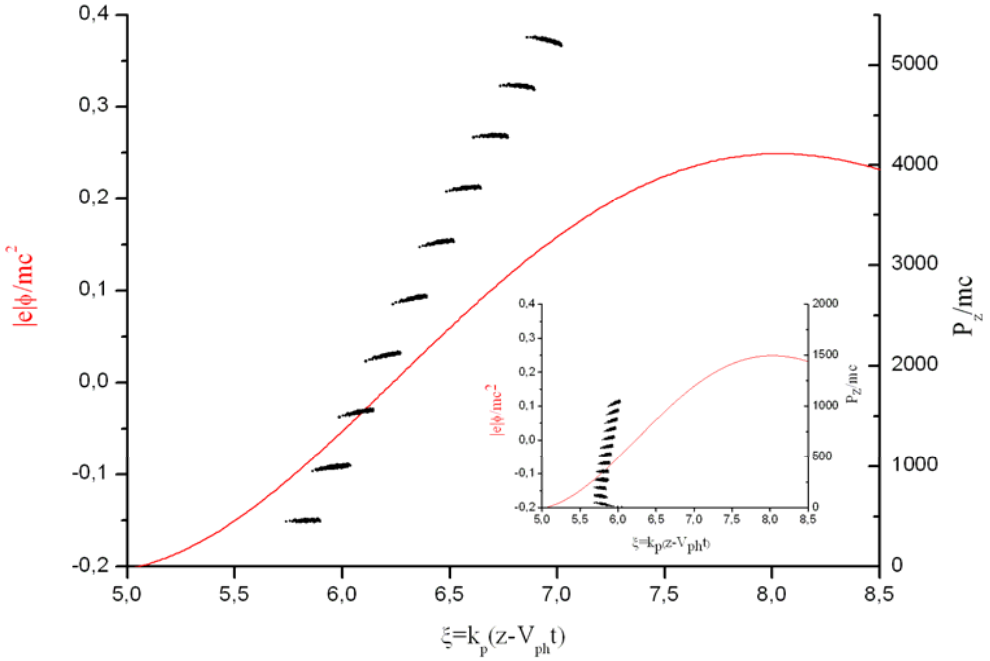

$$E_{inj} = 4.6\ mc^2$$

$$\sigma_{z,inj} = 0.713 k_p^{-1} \approx 120 \mu m$$

$$\sigma_{E,inj} = 1\% E_{inj} = 0.046 mc^2$$

$$E(\xi_f) \approx 2.45\,\mathrm{GeV}$$

$$\Delta E / E(\xi_f) \approx 0.24\%$$

С.В. Кузнецов «Ускорение электронного сгустка, инжектируемого перед лазерным импульсом, генерирующим ускоряющую кильватерную волну» «Физика плазмы», Т. 37, №3, С. 242-256. 2011.

Restrictions on the e-bunch compression

Initial emmitance and loading effect

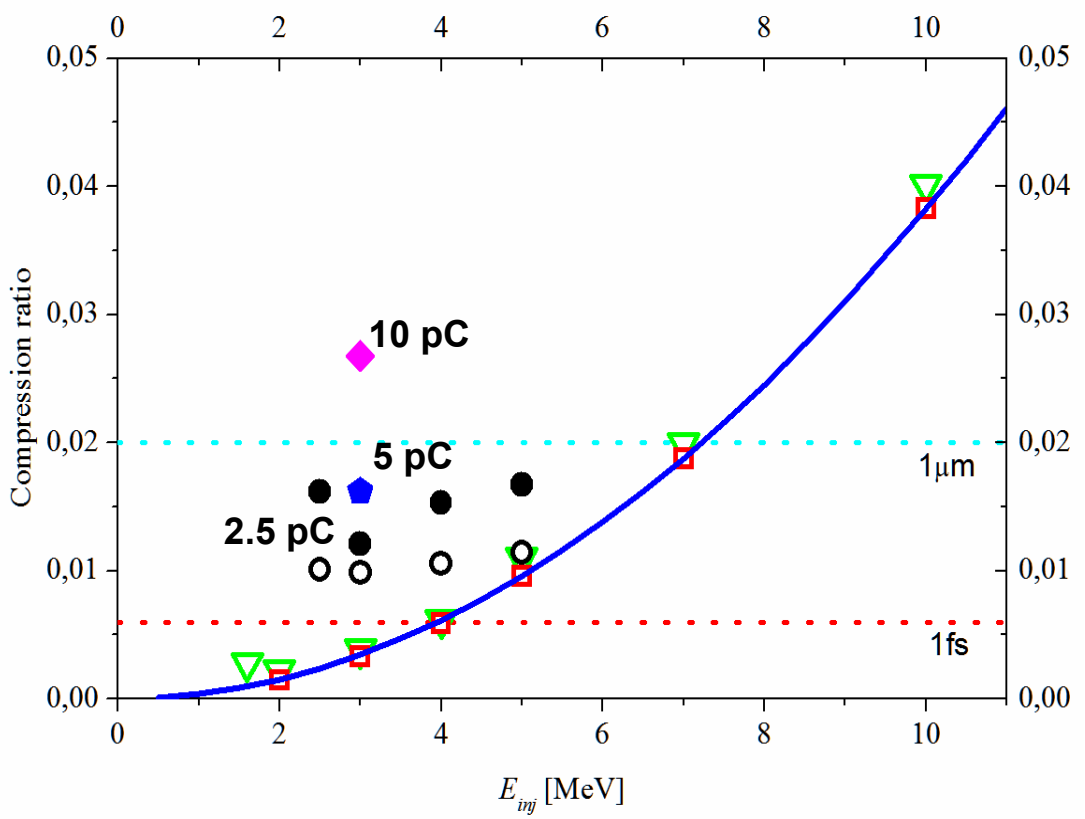

$\gamma_{ph} = 100$

L_{b0}=47μm
R_{b0}=33μm

$\varepsilon_{n0} = 1\,\text{mm}\times\text{mrad}$

open symbols represent 3-D modelling results for the prescribed laser pulse

triangles and squares without loading effect, R_{b0}=2 μm; squares—without influence of ponderomotive force.

Computer simulation by the code LAPLAC

accelerated electron bunch

the bunch has acquired an energy of **2.2 GeV** with a narrow energy spectrum and low emittance 5.4 mm × mrad

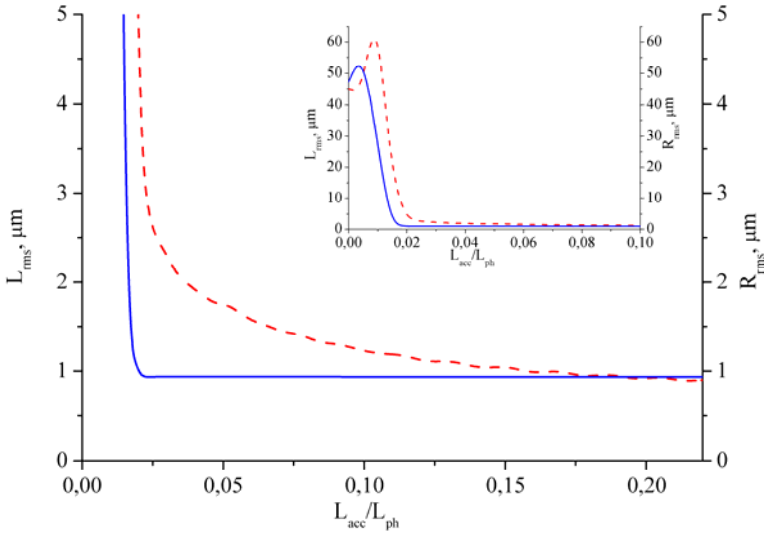

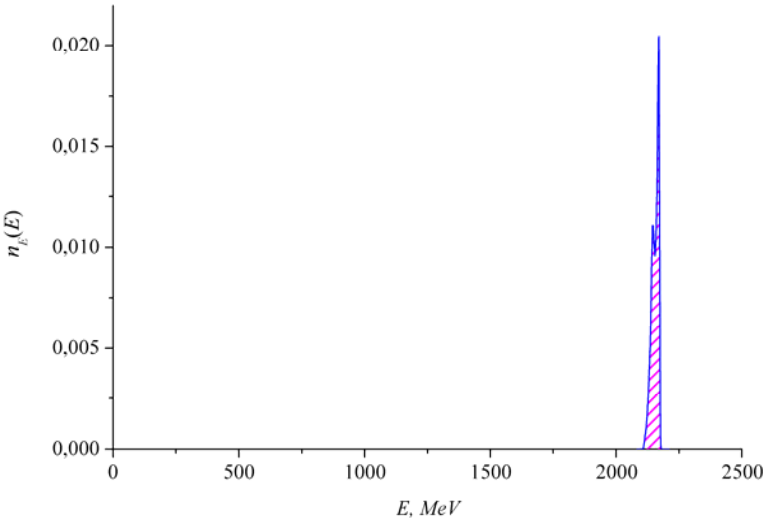

The total trapped and accelerated number of particles in the bunch is about 25% of the injected electrons

$E_{inj} = 3$ MeV $L_{b0} = 2\sigma_z = 47\,\mu$m $r_0 = 37\,\mu$m $I_L = 2.7\times10^{18}$ W/cm^2 $P_L / P_{cr} = 0.35$

Q_b=10 pC R_{b0}=45μm $\tau_{FWHM} = 31$ fs laser energy 2.25 J $n_0(0) = 1.1\times10^{17}$ cm^{-3}

$\varepsilon_{N,r} = 4 r_{rms}\sigma_{P_r/mc} = 1$ mm mrad

$L_b \approx R_b \approx 0.9$ μm

ΔE/E ≈ 1%

N.E. Andreev, V.E. Baranov, B. Cros, V.E. Fortov, S.V. Kuznetsov, G. Maynard, P. Mora, NIM A (2011)

Results of modelling for different injected bunch lengths, charges and radii

q_{inj}, pC	15		10		5		2,5
L_{b0}, μ m	71		47		24		12
R_{b0}, μ m	45	33	45	33	45	33	33
Compression ratio	0.031	0.035	0.019	0.026	0.0177	0.0244	0.0126
Compressed rms length L_b, μm	2.25	2.54	0.93	1.26	0.42	0.58	0.15
Final rms radius R_b, μm	0.98	0.96	0.87	0.85	1.09	0.92	1.06
Final density of accelerated bunch n_b, 10^{18} cm^{-3}	3.3	3.6	5.9	6.8	3.1	3.4	2.7
Trapped charge, pC	3.6	4.6	2.1	3.2	0.77	0.84	0.22
Energy spread ΔE/E, %	8.4	8.0	1.1	2.0	1.4	2.0	1.2
Normalized emittance , ε_n mm×mrad	6.9	6.5	5.4	5.2	8.5	6.3	8.5

Laser pulse transmission in capillary at broken symmetry

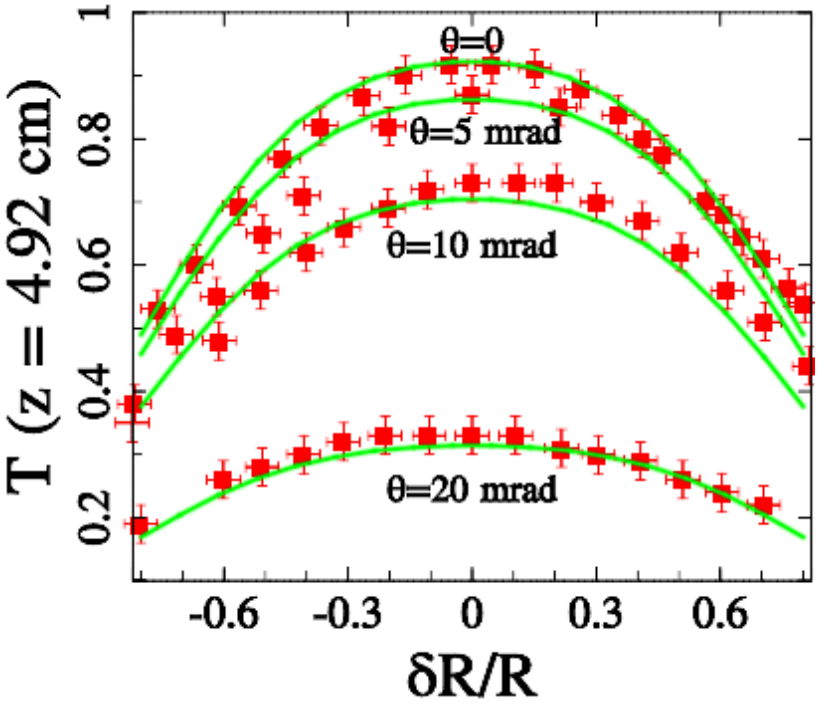

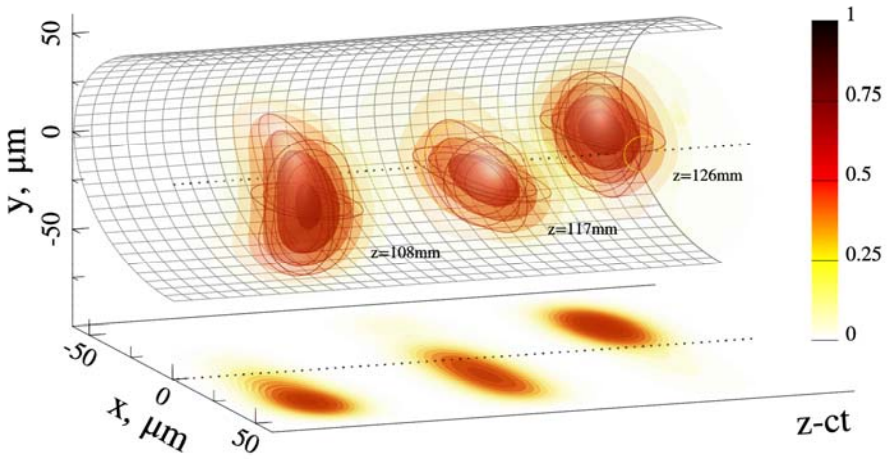

Silicon capillary, $R_{cap} = 51\mu\text{m}$, $r_0 = 32\mu\text{m}$, $\lambda_L = 0.63\mu\text{m}$, circular polarization

linearly-polarized laser pulse with r_0 = 40μm, FWHM duration 135 fs, R_{cap} = 60μm
The angle between laser and capillary axis $\theta = 6\,\text{mrad}$

M.Veysman, N. E. Andreev, K. Cassou, Y. Ayoul, G. Maynard, and B. Cros, J. Opt. Soc. Am. B, V. 27, No. 7 (2010)

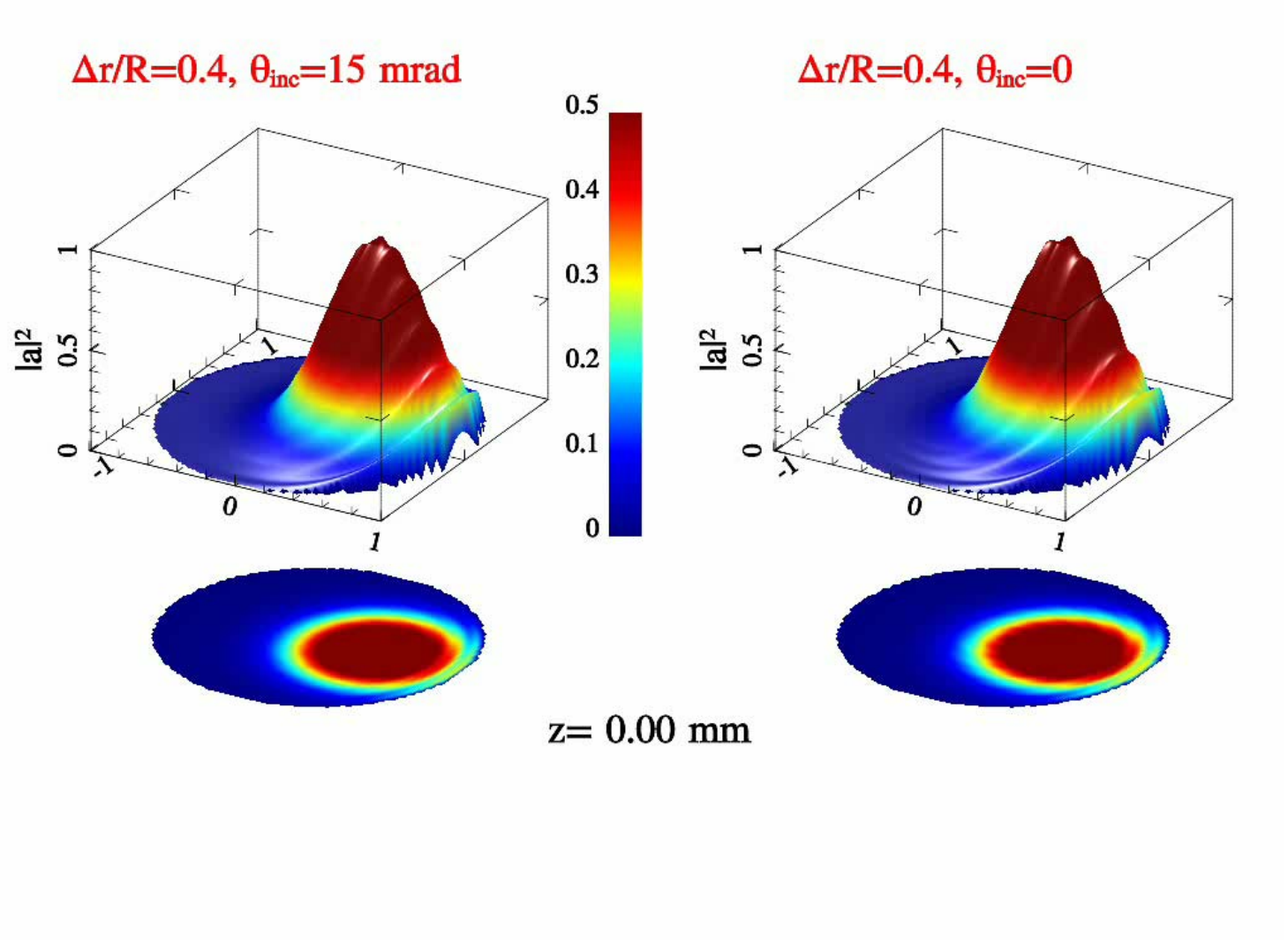

Silicon capillary, $R_{cap} = 51\mu$m,
$R_L = 32\mu$m, $\lambda_L = 0.63\mu$m, circular polarization

Experimental fluence distributions confirm the modelling results

Theory, z=49.5 mm

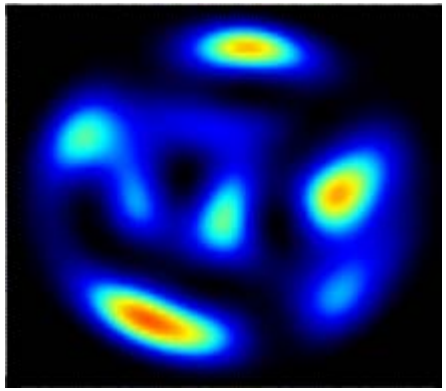

experiment, z=49.5mm

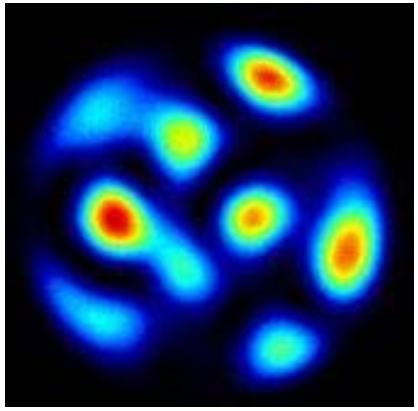

Theory, z=48.5 mm

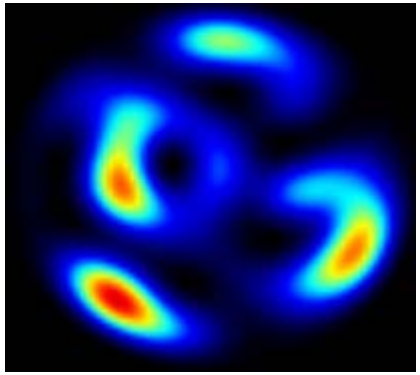

M. Veysman, N.E. Andreev, K. Cassou, Y. Ayoul, G. Maynard, and B. Cros, JOSA B (2010)

When can we reach 1 PeV ?: Suzuki Challenge(2)

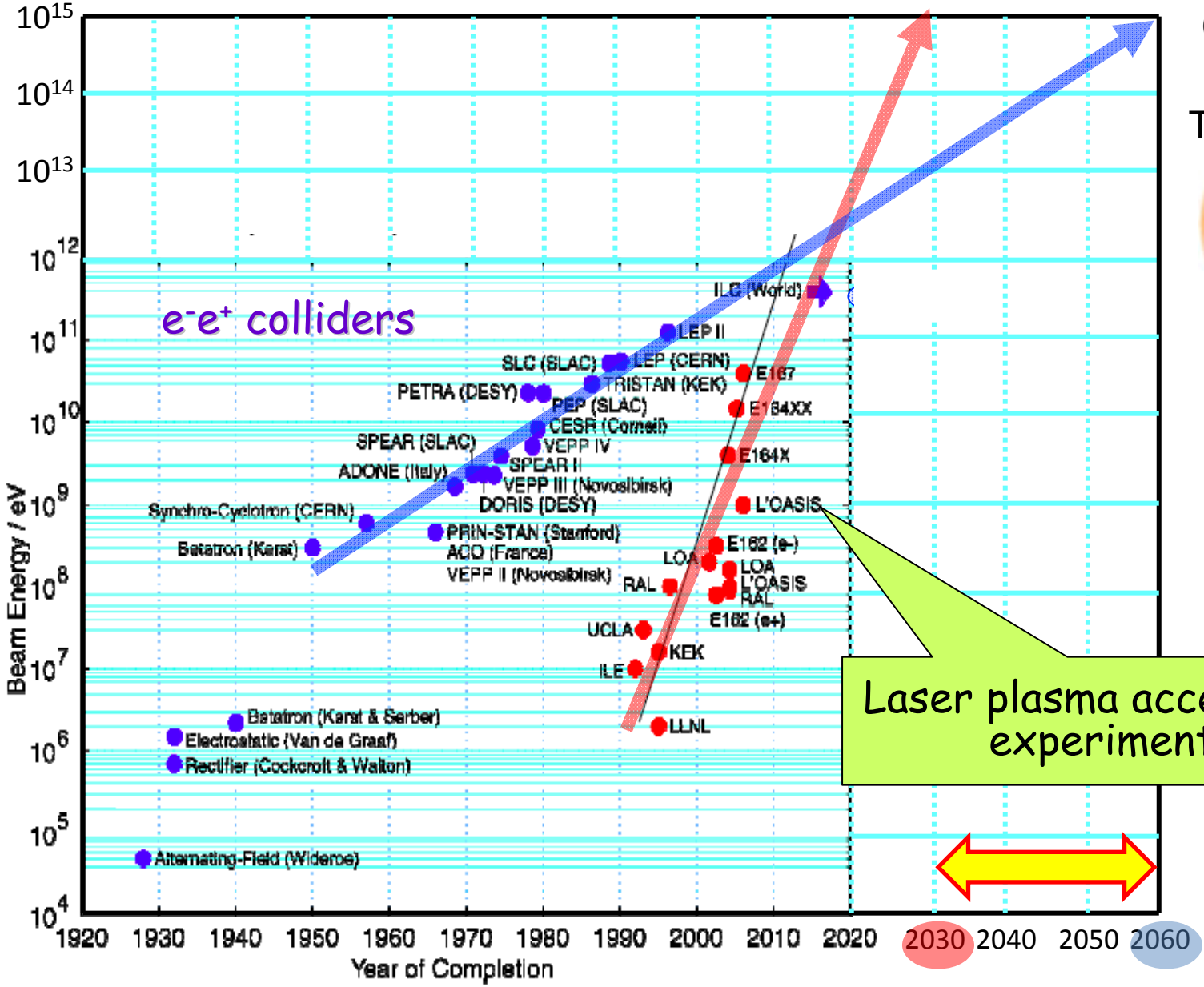

(Suzuki,2009)

Toshi Tajima

ELI Grand Challenges

Paris, April 27th-28th 2009

V. Yakimenko (BNL) and R. Ischebeck (SLAC), AAC2006 Summary report of WG4

With thanks for collaboration to

V.E. Baranov - *Joint Institute for High Temperatures RAS, Russia*
K. Cassou - *CNRS-Universitè Paris XI, France*
B. Cros - *CNRS-Universitè Paris XI, France*
E. Esarey - *Lawrence Berkeley National Laboratory, USA*
V.E. Fortov - *Joint Institute for High Temperatures RAS, Russia*
A.A. Frolov - *Joint Institute for High Temperatures RAS, Russia*
K.V. Khishchenko - *Joint Institute for High Temperatures RAS, Russia*
O.F. Kostenko - *Joint Institute for High Temperatures RAS, Russia*
S.V. Kuznetsov - *Joint Institute for High Temperatures RAS, Russia*
W. Leemans - *Lawrence Berkeley National Laboratory, USA*
P.R. Levashov - *Joint Institute for High Temperatures RAS, Russia*
G. Maynard - *CNRS-Universitè Paris XI, France*
P. Mora - *CPHT, CNRS- Ecole Polytechnique, France*
M.E. Povarnitsyn - *Joint Institute for High Temperatures RAS, Russia*
E.A. Tcirlina - *Joint Institute for High Temperatures RAS, Russia*
M.E. Veisman - *Joint Institute for High Temperatures RAS, Russia*
C-G Wahlström - *Department of Physics, Lund University, Sweden*
F. Wojda - *CNRS-Universitè Paris XI, France*

Спасибо за внимание!